Università degli Studi di Padova

DIPARTIMENTO DI FISICA E ASTRONOMIA "GALILEO GALILEI"

Corso di Laurea Magistrale in Fisica

Tesi di laurea

Criticality in neural networks: a study of the interplay between experimental tools and theoretical models

Relatore:
Prof. Amos Maritan

Correlatore:
Dott. Jorge Hidalgo

Candidato:
Matteo Martinello

Anno Accademico 2015-2016

Contents

Abstract

In the human brain trillions of neurons transmit information "firing" electrical pulses called action potentials or spikes. Neurons are connected to each other and form highly complex networks in which a single neuron may be connected to thousands of other neurons. The activity of single neurons and, more recently, the activity of groups of neurons have been monitored extensively using intracellular and extracellular recordings. One of the most striking observations arisen from such recordings is the fact that neuronal activity seems to be characterized by "avalanches" whose size and lifetime distributions obey a power law, which is typical of self-organized critical systems. Such critical behavior has been confirmed also by theoretical models, but the way avalanches are defined and detected in the experimental analysis is very different from the way they are defined and detected in theoretical simulations. In this work, after a brief review of the concept of Self-Organized Criticality, we describe the experiment that led to the observation of neuronal avalanches. Then, we describe the Millman model, a neuronal network model that reproduces the critical behavior observed in real networks. Finally, we investigate the differences between theoretical and experimental avalanches. In particular, we analyze the data from numerical simulations with the methods used to detect avalanches in real networks. We show that, if the methods of analysis change, the critical behavior is no longer observed.

Introduction: Self-Organized Criticality

The concept of Self-Organized Criticality was introduced for the first time in 1987 by Bak, Tang and Wiesenfeld [1]. They were trying to explain why the $1/f$ noise, i.e. a signal whose power spectral density goes like the inverse of the frequency[1], was so ubiquitous in nature, having been observed in systems as different as the flow of the river Nile, highway traffic and the luminosity of quasars.

To illustrate the concept we can consider the example of the sandpile. Consider a flat table where grains of sand are added slowly at random positions. At first each grain will stay in the same position where it lands; if we continue to add sand, the pile will grow and become steeper and steeper, grains will begin to slide and some of them will hit other grains, causing them to slide too: small avalanches are generated. While in the beginning these slides and avalanches have a local nature and grains at distant parts of the pile do not affect each other, if we continue to add sand we will eventually reach a state where the slope does not increase anymore. In this state there is a balance between the amount of sand added and the amount of sand that leaves the pile falling from the edges: the state is stationary. Also, for the first time there might be avalanches spanning the whole pile: the dynamics stops being local and becomes global. This state is called Self-Organized Critical State.

Bak, Tang and Wiesenfeld made a simple model for the sandpile [2]. They found that in the stationary state the distributions of the avalanche sizes and times obey power laws: the system has no characteristic length scale or time scale. The power law distribution of lifetimes is equivalent to a power law $1/f$ frequency spectrum, that is what Bak, Tang and Wiesenfeld were trying to explain in the first place.

The absence of a characteristic scale is typical of critical phenomena. In the Ising Model, for instance, there are two distinct phases; the disordered phase, with zero magnetization, occurs when the temperature is higher than the critical temperature while the ordered phase, with non zero magnetiza-

[1]Spectra going like $1/f^{\alpha}$ instead of $1/f$ are also commonly referred to as $1/f$ noise.

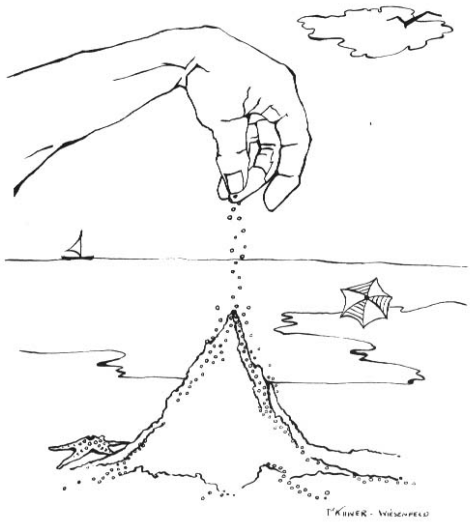

Figure 1: Sandpile. Drawing from Bak, 1996 [3].

tion, occurs when the temperature is lower than the critical value. At the critical temperature the two phases coexist and there are ordered domains of all sizes: there is no characteristic size, just like for the avalanches in the sandpile model.

Despite the analogies, a self-organized critical state is very different from the state of a system at the phase transition in equilibrium statistical mechanics; in fact, in the Ising Model the critical point can be reached only by accurately tuning a parameter, the temperature, while the self-organized critical state is an attractor for the dynamics: self-organized critical systems naturally evolve to the critical state without anybody tuning the parameters. To see this, let us consider the example of the sandpile once again; if we start adding sand to a flat table the pile will became steeper and steeper and eventually will reach the critical point; on the other hand, a pile that is too steep will collapse and eventually it will reach the critical state too. In both cases, once in the critical state, the system will stay there: the state is an attractor for the dynamics.

One of the consequences of operating at the self-organized critical state is the fact that catastrophic events occur with a well defined probability and are generated by the same mechanisms that generate smaller events. Furthermore, most of the changes do not happen gradually but as a consequence of such catastrophic events [3].

It has been suggested that Self-Organized Criticality is the underlying mechanism governing the dynamics of phenomena as diverse as, for instance, earthquakes [4], forest fires [6] and solar flares [7]. In fact, such phenomena

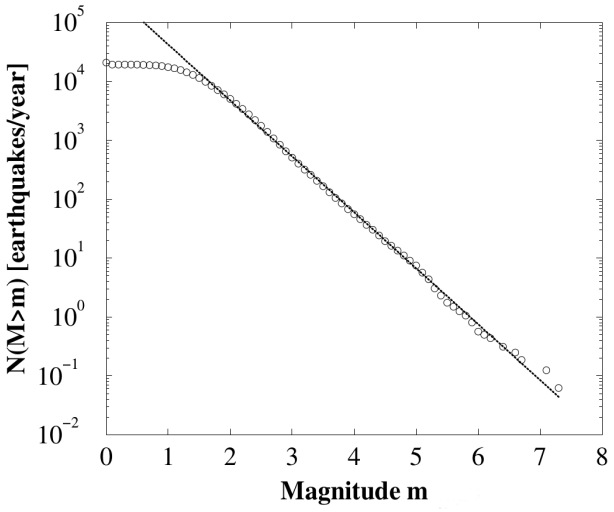

Figure 2: Distribution of the number of earthquakes N with a magnitude M larger than m per year as a function of m. Since the magnitude m is related to the logarithm of the energy E released during an earthquake, the distribution is equivalent to a power law, which is a signature of criticality. The dashed line is known as the Gutenberg-Richter law. Data relative to California and to the period 1984-2000. The plot is in lin-log coordinates. Plot from Bak et al., 2002 [5].

are characterized by scale invariant distributions (see figures 2, 3 and 4) that have been reproduced modeling them as self-organized critical phenomena.

Even though at first Self-Organized Criticality was applied only to systems of inanimate matter, the theory was soon extended to biological systems. For instance, it has been suggested that cellular states self-organize in a critical state where they achieve optimal growth [9]; also, it has been suggested that flocks of birds self-tune into a critical state where they are able to react collectively to external perturbations such as predatory attacks [8]. Similar conclusions, supported by empirical evidence, have been drawn for bacterial clustering [10], morphogenesis [11], gene expression patterns [12] and many other biological systems, leading to the suggestion that living systems might operate at or near a critical point [8].

An important example of Self-Organized Criticality in living systems is given by neural networks. Neurons are electrically excitable cells that respond to electrical and chemical inputs by generating electrical signals and transmitting them to other cells. Such electrical signals are called action potentials or spikes. Neurons are connected to each other through synapses and form highly complex networks in which a single neuron may be connected to thousands of others. When a neuron fires an action potential, such a signal

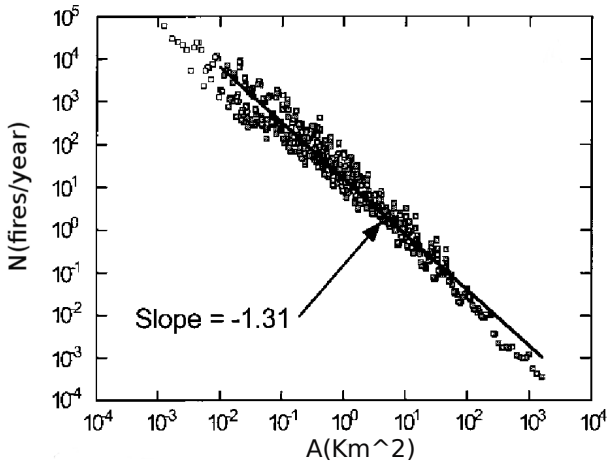

Figure 3: Distribution of the number of fires per year N as a function of the fire area A. The distribution follows a power law, which is a signature of criticality. Data relative to U.S. Fish and Wildlife Service lands and to the period 1986–1995. The plot is in log-log coordinates. Plot from Malamud et al., 1998 [6].

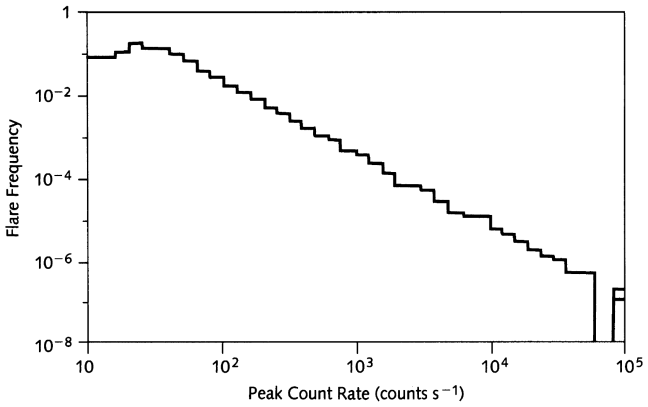

Figure 4: Distribution of solar flares frequency as a function of solar flares intensity (given by the peak count rate). The distribution follows a power law, which is a signature of criticality. Measurements are taken by the NASA satellite ISEE3/ICE. The plot is in log-log coordinates. Plot from Bak, 1996 [3].

travels along synapses and may excite some of the postsynaptic neurons, making them fire too. This mechanism might start a chain reaction, causing many neurons to fire an action potential; this cascade of activity is called a neuronal avalanche. The existence of neuronal avalanches was observed experimentally by Beggs and Plenz [13] and, remarkably, the distribution of their sizes was found to follow a power law, which is a signature of criticality. This reminds us of the sandpile, where activity occurs in avalanches whose size is given by a power law. The observation of neuronal avalanches led to the suggestion that the brain self-organizes in a critical state at the boundary between being almost dead and being fully epileptic [8]. This can be explained with the help of the branching parameter σ, which is defined as the average number of neurons connected to a neuron that has fired that, in turn, fire. If $\sigma < 1$ avalanches are small and last for a short time so that each signal is attenuated and cannot be transmitted efficiently: the brain is almost dead. On the contrary, if $\sigma > 1$ avalanches grow unlimitedly in size and lifetime causing a runaway activation of the brain that leaves little information of the original signal: the brain is epileptic. If $\sigma = 1$, on the other hand, there are avalanches of all sizes and durations: the system is at the critical point and information can be transmitted efficiently. Beggs and Plenz measured the branching parameter σ of a network of cortical neurons and found it to be around the critical value $\sigma \approx 1$ [13].

The critical behavior of the brain has been reproduced by theoretical models. One of such models is the Millman model, which reproduces both the power law behavior of avalanche size distribution and the critical value of the branching parameter. However, the way avalanches are defined and detected in the experimental analysis is very different from the way they are defined and detected in theoretical simulations. This is due to the fact that, while in theoretical simulations we can get all the information we need about the system, the information we can obtain from experiments is always partial.

In the first chapter of this work we discuss the methods by which Beggs and Plenz were able to detect neuronal avalanches. In the second chapter we give an overview of the general properties of neurons and of neuronal dynamics. In the third chapter we describe the Millman model and its predictions, and in particular the prediction of the existence of neuronal avalanches whose size is given by a power law. In the last three chapters we investigate the differences between the avalanches observed by Beggs and Plenz and the ones simulated by the Millman model; in particular, we analyze the data from numerical simulations with the methods used to detect avalanches in real networks. We show that, if the methods of analysis change, the critical behavior is no longer observed.

Chapter 1

Criticality in neural networks: experimental evidence

The existence of neuronal avalanches with sizes distribution following a power law was reported for the first time by Beggs and Plenz [13] in 2003. In this chapter we present their work, focusing on the methods of experimental analysis that led to the observation of avalanches.

1.1 Experimental set-up

In order to study the propagation of neuronal activity, brain slices were removed from the somatosensory cortex and the primary motor cortex of a group of rats. The somatosensory cortex is a brain area that responds to somatic stimuli, while the primary motor cortex is one of the areas in charge of planning and executing movement. Two types of brain slices were prepared: cultured and acute slices. The former can be mantained in vitro for a long time (from weeks to months) and require a more complex preparation, the latter require an easier preparation and are usually used on the same day when they are prepared.

Neuronal activity was monitored placing the slices on a 64 multielectrode array (see figure 1.1). Each electrode was embedded within the brain slice and recorded the voltage variation in the extracellular area close to it. The signal generated by this voltage variation is called Local Field Potential (LFP) and typically consists of a sharp negative peak [14] (see figure 1.1). Both experimental evidence [15][16] and numerical simulations [17] suggest that LFPs represent a synchronized action potential emission from the neurons in the vicinity of the electrode.

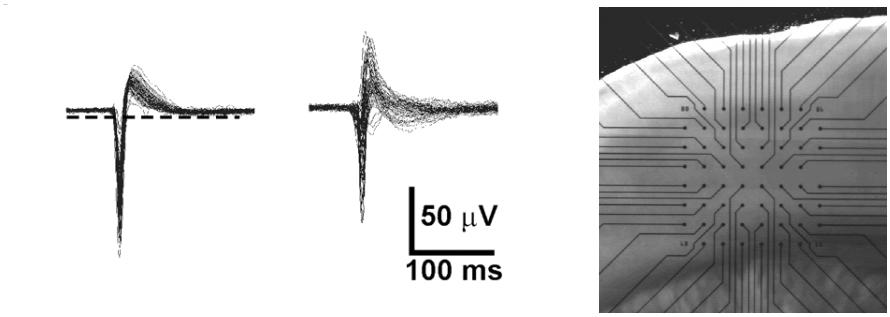

Figure 1.1: Left: Local Field Potentials; superposition of LFP's at the same electrode (left) and superposition of LFP's at different electrodes (right). Right: Acute slice on the mulielectrode array; the distance between an electrode and its nearest neighbor is of $200\mu m$. From Beggs and Plenz, 2003[13].

1.2 Experimental analysis - cultured slices

The analysis of seven cultured slices, based on the data extracted from a total of 70 hours of recording, showed brief periods of synchronized bursts of activity, where LFPs were recorded simultaneously by many electrodes, separated by longer periods of quiescence, where no LFPs were recorded. The active periods lasted $\sim$ 100 ms, while the quiet periods were of the order of seconds. At the time when Beggs and Plenz published their work this behavior had been already observed in cultured slices (see for instance Plenz and Aertsen, 1996 [20]).

Beggs and Plenz studied the temporal correlation between signals recorded by different electrodes during an active period and realized that the synchrony of the LFPs was only apparent; in fact, even though the LFPs recorded by different electrodes during the active periods looked like they were occurring at the same time, a more accurate analysis made by looking at the data at a higher temporal resolution, suggested that the apparent synchrony of the LFPs was hiding more complex spatiotemporal patterns (see figure 1.2).

1.2.1 Neuronal avalanches

In order to investigate the nature of these spatiotemporal patterns, Beggs and Plenz processed the signal from each electrode. A threshold was fixed and an event was associated to each LFP that crossed the threshold. For each event the amplitudes of maximum excursion from the threshold and the corresponding times were recorded.

The threshold was obtained plotting the receiver operating characteristic curve given by the data and a Gaussian distribution representing the noise (see Appendix for an explanation of the receiver operating characteristic

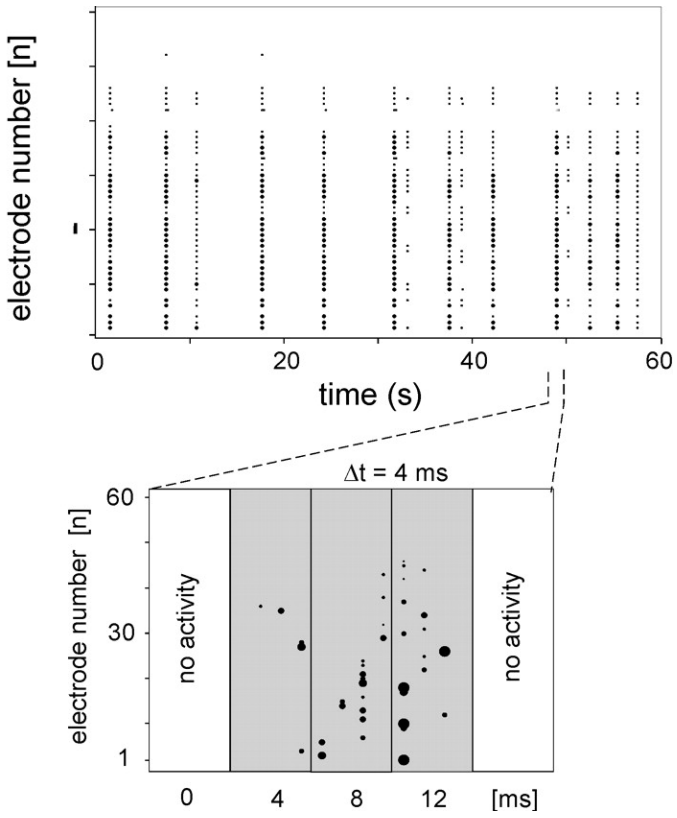

Figure 1.2: Actity during active periods. When active periods are analyzed at higher temporal resolution, complex spatiotemporal patterns emerge. Plots from Beggs and Plenz, 2003 [13].

analysis) [18][19].

Once events were defined and searched for in the data, the spatiotemporal patterns formed by these events were studied. A time interval Δt was used to bin the data and for each time bin the number of events was counted. A sequence of successive time bins with at least one event that was preceded and ended by an empty bin was called an avalanche.

1.2.2 The power law

The size of an avalanche was expressed in two different ways, as the number of events and as the sum of the amplitudes associated to each event of the avalanche. In both cases the distribution of sizes was shown to obey a power law

$$P(s) \sim s^{\alpha} \tag{1.1}$$

where s is the size of an avalanche, given by one of the two previous definitions, and $P(s)$ is the probability of finding an avalanche of size s. The exponent α was approximately the same in both cases. The existence of such a power law became even clearer after plotting the size distribution in log-log coordinates, where the power law gives rise to a linear relation between the coordinates, where the slope is given by the exponent α of the power law.

When the first definition of avalanche size was used, the plot showed a cutoff around ~ 60 (see figure 1.3), which is approximately the number of electrodes used for the recording; this suggested that, during an avalanche, most of the electrodes do not register more than one event.

1.2.3 Interevent interval (IEI)

Even though the power law seemed to describe correctly the size distribution, having been found using two different size definitions, both of them giving the same exponent α, a problem soon arose. In fact, when the same analysis was made using a different Δt to bin the data, although the power law behavior was confirmed, different values of the exponent α were found: the slope turned out to be dependent on Δt (see figure 1.3). In particular, bigger Δt values resulted in a power law with a more gradual slope, while smaller Δt gave a power law with a steeper slope. This can be explained in this way: a longer time interval will put together events that were placed in different avalanches, resulting in more big avalanches and less small ones (the slope becomes more gradual); on the contrary, a smaller time interval will put in different avalanches events that were placed in the same one, resulting in less big avalanches and more small ones (the slope becomes steeper).

The dependence of the slope on the time interval raised some questions about the nature of α. Was the exponent a true feature of neuronal networks or was it just a mathematical artifact without any physical meaning? In order to answer this question Beggs and Plenz defined the average interevent

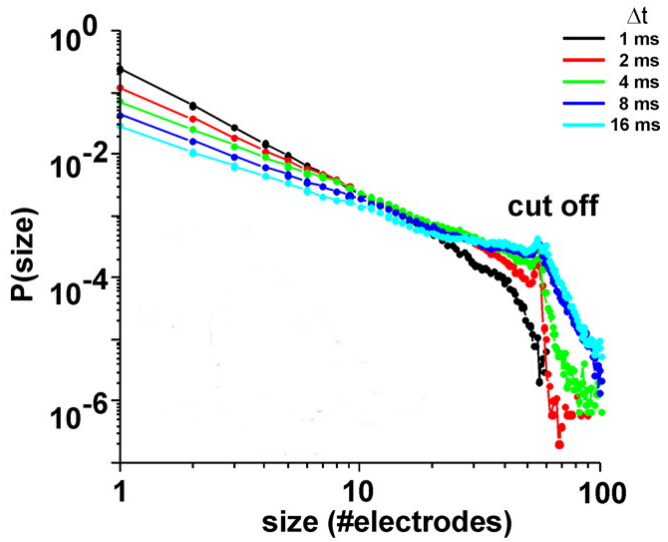

Figure 1.3: Actity during active periods. Avalanche size distributions calculated using different Δt to bin the data. Different Δt give rise to different slopes. The plot is in log-log coordinates. Avalanches are expressed as the number of events. Plots from Beggs and Plenz, 2003 [13].

interval (IEI) as the average time interval between successive events of the same active state: for each burst of activity they measured the time interval between each event and the following one and took the average. They measured the IEI for each of the seven cultured slices, then they binned each set of data using the respective IEI and plotted the results. They found that, even though the IEIs were different for each culture, all the size distributions had the same slope; the value of the exponent they observed was

$$\alpha = -1.50 \pm 0.008 \ .$$

This observation led to the suggestion that the data had to be binned with a specific time interval, which was precisely the interevent interval. Furthermore, it suggested that the exponent $-3/2$ was the characteristic exponent of the system.

1.2.4 Array rescaling

In order to give further evidence to support the choice of the IEI as the correct time interval to be used in the binning, Beggs and Plenz studied the system using only the data recorded by some subsets of the electrodes.

The distance between an electrode and its nearest neighbor was of 200 μm; such distance was called interelectrode distance (IED). Beggs and Plenz se-

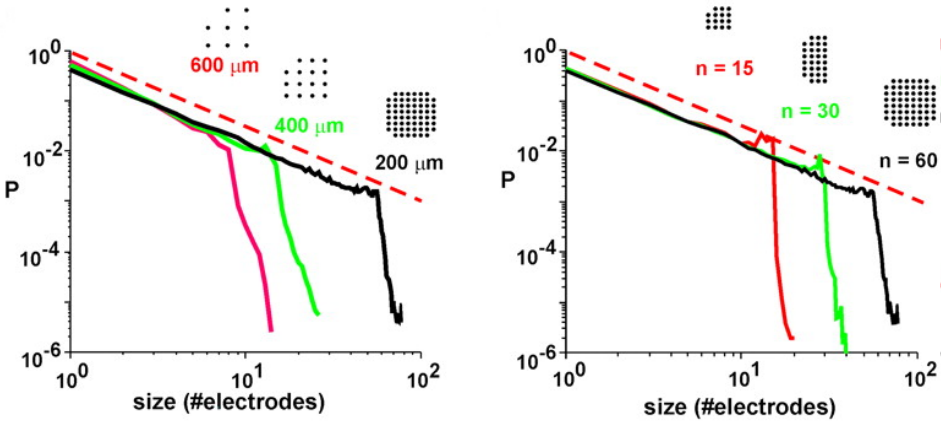

Figure 1.4: Array rescaling. On the left: size distributions obtained changing the IED. On the right: size distributions obtained cutting the array in halves and in quarters. In both cases, the slope does not change. The plot is in log-log coordinates. Avalanches are expressed as the number of events. Plots from Beggs and Plenz, 2003 [13].

lected from the original 8 by 8 array with IED of 200 μm a 4 by 4 array with IED of 400 μm and then a 3 by 3 array with IED of 600 μm. For each of these subsets they calculated the IEI and used it for the analysis. They found that, even though the lower number of electrodes resulted in a bigger IEI, and even though the IED had changed, the observed value of the exponent was still $\alpha \sim -3/2$ (see figure 1.4). The independence of the exponent from the rescaling of the array supported the validity of the methods of analysis used to classify the avalanches; furthermore, it supported the hypothesis that $-3/2$ was indeed the characteristic exponent of the system.

An additional test was made by changing the threshold used to select the events: the analysis made using a wide range of thresholds did not change significantly the slope of the size distribution.

Since the size distribution showed a cutoff around the number of electrodes in the array, the array was divided in halves and the analysis was performed using only the electrodes in one of the halves; the same was done dividing the array in quarters. This selections had a diminished number of electrodes, but the same IED as the complete array. The analysis showed that the cutoff was dependent on the number of electrodes (see figure 1.4), leading to the suggestion that an infinite array would give no cutoff.

1.2.5 Lifetime distribution

In addition to the size distribution, the lifetime distribution was studied too. For a fixed Δt used for the binning, the lifetime of an avalanche was

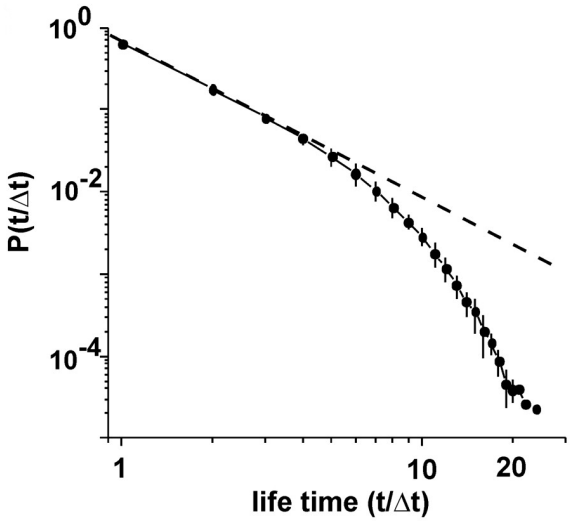

Figure 1.5: Scale invariant function given by rescaled lifetime distributions. The function initially obey a power law with slope -2 (dashed line), then exhibit an exponential cutoff. Plots from Beggs and Plenz, 2003 [13].

defined as the number of time bins of the avalanche times Δt. The lifetime distribution was shown to obey a power law with an exponential cutoff (see figure 1.5). Furthermore, different values of Δt did not change the shape of the distribution. In order to compare distributions given by different bin widths, each distribution was rescaled using the transformation

$$t \to t/\Delta t \ .$$

The rescaled distributions were plotted together and were shown to collapse into a unique, scale-free, function. The first part of this function was described by a power law with exponent $\alpha \sim -2$ (see figure 1.5).

1.2.6 Activity propagation

The observation that LFPs at different electrodes did not occur at the same time suggested that neuronal activity might spread from an electrode to the others. In order to investigate the propagation of such activity a contiguity index I was defined. For each electrode that had registered an event during a time bin, the previous time bin was searched for events registered by his neighbors electrodes. The contiguity index was defined as the fraction of events preceded by an event at neighbors electrodes.

The analysis of cultured slices gave a contiguity index of:

$$I = 39.3 \pm 8\% \ ,$$

showing that activity propagation in cultured slices is very different from a wave-like propagation, that would result in a 100% contiguity index.

1.3 Experimental analysis - acute slices

In order to prove that the results obtained from the analysis of cultured slices were not an outcome of culture preparation, the same analysis was carried out on a set of acute slices. The size distribution showed the power law behavior already observed in the cultures; furthermore, the value of the exponent was observed to be still $\alpha \sim -3/2$. The main difference was the fact that in acute slices most of the avalanches were not made by more than ten events; this might be a consequence of the fact that the slicing process reduces the connectivity between distant parts of the slice and, while cultured slices have the time to rebuild it, acute slices do not. As in the case of the cultures, the lifetime distribution was found to be initially following a power law with exponent $\alpha \sim -2$ and than relaxing with an exponential cutoff.

1.4 Criticality

The observation of the exponents $-3/2$ and -2 in the power law distributions of sizes and lifetimes was very intriguing; in fact, these are the same exponents predicted by the theory for a critical branching process.

1.4.1 The theory of branching processes

The theory of branching processes goes back to 1874 and to the work of Galton and Watson [22], who wanted to prove wrong an hypothesis that was common at the time, the idea that distinguished families were more likely to extinguish than ordinary families. A branching process can be explained in terms of ancestors and descendants. Each ancestor can give birth to $n \in (0, 1, 2, ..., \infty)$ descendants with probability p_n and each descendant can, in turn, give birth to n descendants with the same probability. The critical behavior can be investigated by means of the branching parameter σ, that is defined as the average number of descendants per ancestor [23]:

$$\sigma = \sum_{n=0}^{\infty} n p_n \ . \tag{1.2}$$

It can be proved [22] that if $\sigma = 1$ the branching process becomes critical and the distribution of the total number of descendants in each generation obeys a power law with exponent $-3/2$.

The theory of branching processes was developed during the twentieth century and, in particular, its connection with self-organized criticality was investigated, leading to the suggestion that a critical branching process could describe the dynamics of sandpile models.

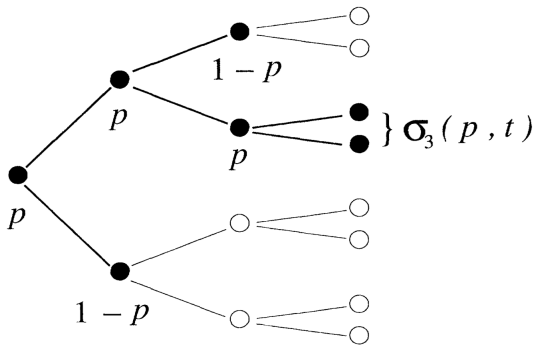

Figure 1.6: Drawing of an avalanche in a system with a maximum of $n = 3$ generations. Black sites correspond to events and form an avalanche of size $= 7$, with $\sigma_3 = 2$ events of third generation. The avalanche is drawn on a tree of dimension $N = 15$. Drawing from Zapperi et al., 1995[21].

1.4.2 Self-organized branching processes

In this section we describe the self-organized branching process (SOBP) [21], a theory that connects the theory of self-organized criticality and the theory of branching processes. In particular, we show that the exponents predicted by such a theory are exactly the ones found by Beggs and Plenz. We will see that, while the ordinary theory of branching processes requires the tuning of the branching parameter σ to become critical, the SOBP naturally evolves to the critical point without the need for an external tuning; therefore, such a theory seems more fit to be compared to a biological system such as a neural network, where no external tuning is performed.

In the SOBP an avalanche starts with an event (the ancestor); there is a probability p that such an event will lead to two new events (two decendants) and a probability $1 - p$ that the avalanche will stop. Boundary conditions set the maximum number of generations in an avalanche to n, so that each avalanche can be described using a tree of size $N = 2^{n+1} - 1$ (see figure 1.6). An avalanche can or cannot reach the boundary depending on whether or not there are events of n-th generation. Let us call the number of such events σ_n. In the SOBP the probability p is a dynamical variable whose value, after each avalanche, changes according to the equation:

$$p(t+1) = p(t) + \frac{1 - \sigma_n(p,t)}{N} \ . \tag{1.3}$$

In order to explain this equation, let us consider the sandpile once again. When the slope is less steep than the critical slope, the amount of sand added to the system is more than the amount that leaves the sandpile falling from its edges. In this situation, the slope grows steeper and the probability

of large avalanches increases with increasing slope. On the contrary, when the slope is steeper than the critical value, the amount of sand that leaves the system is bigger that the amount added to the sandpile. In this situation, the slope becomes more gradual and the probability of large avalanches decreases with decreasing slope. The number of events of n-th generation in the SOBP can be thought of as the sand that leaves the sandpile: as in the sandpile, after a big avalanche which causes a lot of sand to leave the system (and the slope to decrease), the probability of large avalanches decreases, in SOBP an avalanche with a lot of events of n-th generation causes the probability p to decrease; on the contrary, an avalanche with no events of n-th generation causes the probability p to increase.

Knowing that, for a fixed p, the average of σ_n is given by [22]

$$\langle \sigma_n(p,t) \rangle = (2p)^n \ ,$$

we can write $\sigma_n(p,t) = (2p)^n + \eta(p,t)$, where η represents the fluctuations around the average. Substituting in (1.3) we find

$$\frac{dp}{dt} = \frac{1-(2p)^n}{N} + \frac{\eta(p,t)}{N} \ . \tag{1.4}$$

Ignoring the last term, which becomes negligible in the limit $n \longrightarrow \infty$, we can see that $p = 1/2$ is a fixed point for equation (1.4) and that such fixed point is an attractor for the dynamics. $p = 1/2$ is the critical value of the branching process; in fact, in the limit $n \longrightarrow \infty$ it is at the boundaries between $p < 1/2$, where all the avalanches are finite, and $p > 1/2$, where there is a non-zero probability of observing an infinite avalanche. At the critical point, as we will see, avalanches of all sizes are present and their distribution follows a power law. The fact that the critical point is an attractor for the dynamics shows that the model describes a self-organized critical system. This has been verified by numerical simulations showing that, no matter what the initial values of p are, the system self-tunes around the critical point with $p = 1/2$. Furthermore, numerical simulations for the system at the critical point show that the size distribution and the lifetime distribution of the avalanches follow a power law with exponents $\alpha \sim -3/2$ and $\alpha \sim -2$ (the lifetime of an avalanche has been defined as the number of generations). The same results can also be obtained analytically [21].

The branching parameter σ introduced in the previous section can be calculated also for a SOBP. In this process, at the critical point, each ancestor can only have two descendants with probability 1/2; this gives the value $\sigma = 1$ for the branching parameter, as predicted for a critical branching process.

1.4.3 The branching parameter in neural networks

The observation that the exponents given by the analysis of neural networks were the same exponents of the critical branching process suggested that

the critical branching process was the mechanism governing the dynamics of neural networks. In order to investigate this matter Beggs and Plenz introduced a definition of the branching parameter that was fit for their system [13]. They looked for the avalanches with only one event in the first time bin and counted the events in the second time bin. They defined the branching parameter σ as the average number of events in the second time bin of the avalanches started by a single event. They also extended this definition to take into account the avalanches with more than one event in the first time bin. For such avalanches σ was measured taking the average of

$$\text{round}\Big(\frac{\text{events in the second bin}}{\text{events in the first bin}}\Big) \ .$$

The branching parameter was measured from the cultures data processed using the IEI for the binning and taking into account all the electrodes. The values observed were:

$$\sigma = 1.04 \pm 0.19$$

for the avalanches with one event in the first bin and

$$\sigma = 0.90 \pm 0.19$$

taking into account all the avalanches. The lower value observed in the second case can be explained considering that if an avalanche is started by multiple events (at different electrodes) it might happen that two of this events trigger an event at the same electrode, resulting in an underestimation of σ. Furthermore, it has been observed that typically an LFP crosses over the threshold for 20 ms before crossing back, so that an electrode registers no more than one event in a time interval of 20 ms; then, if an avalanche is started by multiple events, the number of electrodes that can register an event in the second time bin is reduced, leading, again, to a lower estimation of σ.

In order to verify that the observation of the critical value $\sigma \sim 1$ was truly a consequence of the temporal patterns of activity typical of cultured cortical networks, Beggs and Plenz altered the LFP times of 50 data sets; each event was randomly moved 4 ms forward or backwards in time and then the branching parameter was measured from the new sets of data. The analysis gave a branching parameter $\sigma \sim 0.7$. σ was also measured from sets of data altered using bigger translations, up to 80 ms. The analysis showed that the more the data had been altered, the more the branching parameter had moved away from the critical value.

At last, the system was binned using five different time intervals and for each interval both the branching parameter σ and the exponent of the size distribution α were measured. The five couples of values correspond to five points in the (σ, α) plan and these points can be used to calculate a trajectory for the values of σ and α as a function of the time interval used

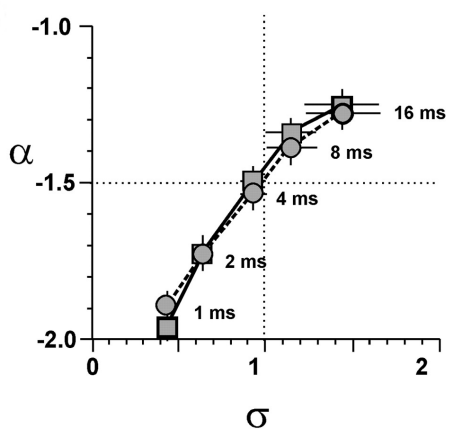

Figure 1.7: Trajectory for the values of σ and α as a function of the time interval used in the binning. The trajectory crosses through the point $(1, -1.5)$ at the time interval $\Delta t \approx 4\ ms$, close to the interevent interval IEI $= 4.2\ ms$. Circles: avalanche size calculated as the number of events; squares: avalanche size calculated as the sum of amplitudes. Plots from Beggs and Plenz, 2003[13].

in the binning. The trajectory calculated in this way by Beggs and Plenz crosses through the point $(1, -1.5)$ and, furthermore, the crossing occurs at the time interval $\Delta t \approx 4\ ms$, which is very close to the interevent interval IEI $= 4.2\ ms$ (see figure 1.7). This result is a further confirmation of the fact that using the IEI to bin the data leads to the value $-3/2$ for the slope in the size distribution.

1.5 Conclusions

The analysis that Beggs and Plenz made on cultured and acute slices led to the observation of neuronal avalanches whose sizes and lifetimes are described by a power law. Since the exponents observed in this power laws were the same predicted by the theory for a critical branching process, it was suggested that the critical branching process could be the mechanism governing the dynamics of the system. This was also tested by measuring the branching parameter σ, that turned out to be set around the critical value $\sigma = 1$, at the boundary between a runaway activation of the network ($\sigma > 1$) and a state where neural activity decreases over successive steps ($\sigma < 1$). In particular, the fact that the system approaches the critical point without an external tuning suggested that the system could be a self-organized critical system.

Chapter 2

Neuronal dynamics

In this chapter we give an overview of the general properties of neurons and of neuronal dynamics. Also, we introduce the integrate-and-fire model, a simple but widely used neuron model. The reader who is already familiar with such subjects can skip this chapter an go on to the next one.

2.1 Properties of neurons

Neurons are electrically excitable cells that respond to electrical and chemical inputs by generating electrical signals and transmitting them to other cells [25]. The connections through which neurons transmit and receive signals are called synapses. Typically, neurons consist of three parts: the soma, the dendrites and the axon (see figure 2.1). The soma is the body of the neuron and contains the nucleus, dendrites are branched structures that arise from the soma and receive the signals from other neurons while the axon is a cellular extension that carries signals from the neuron to other cells.

To get an idea of the orders of magnitude involved, the diameter of the soma of a cortical neuron ranges from 10 to 50 μm; the study of cortical neurons of the mouse brain has showed that about 40 mm of axon and 4 mm of dendrites come out of the soma of such neurons; on average, there are 180 synaptic connections per mm along an axon and 2 per μm along dendrites.

2.1.1 Electrical properties

Neurons contain a huge number of charged particles, such as Na^+, K^+, Ca^{2+} and Cl^- ions (typically, a cubic micron of cytoplasm contains 10^8 ions). Usually there is an excess of negative charge inside the neuron, resulting in a negative potential difference between the neuron and the extracellular medium, whose potential is conventionally set to zero. Such potential difference is called membrane potential and his rest value is usually around

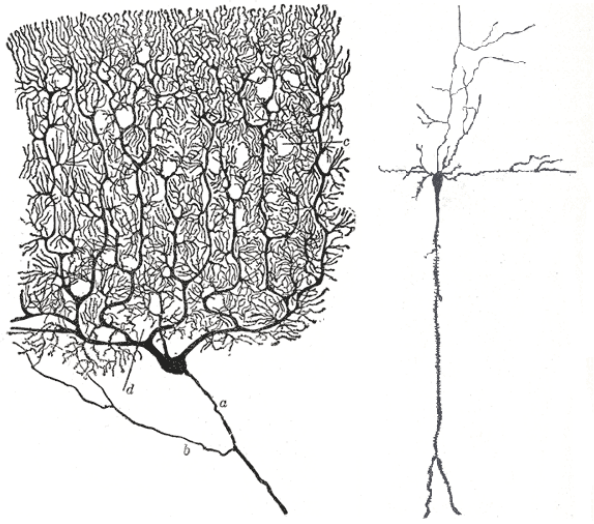

Figure 2.1: Drawings of two different neuronal cells. On the left, the cell of Purkinje from the cerebellum, on the right, a pyramidal cell from the cerebral cortex of a mouse. On the upper part of each drawing there is the dendritic tree, on the lower part there is the axon.

$-70\ mV$.

The cell membrane separates the inside of the neuron from the extracellular fluid surrounding it. Charged particles can cross the cell membrane passing through ion channels that can open and close in response to voltage variations, variations in the concentration of some types of ions inside the cell and variations in the concentration of neurotransmitters in the extracellular medium. Most of the ion channels allow only a single type of ion to cross the membrane, even though there are also channels that are not so selective. The concentration of ions is different inside and outside the neuron because of the action of ion pumps, located in the membrane potential.

In order to investigate the electrical properties of neurons it is useful to introduce the definitions of membrane capacitance and membrane resistance [24]. The membrane capacitance can be explained in this way: the excess of negative charge inside a neuron causes negative ions, that repel each other due to electrostatic forces, to gather on the interior surface of the cell membrane, causing an equal amount of positive charge to gather on the exterior surface. Therefore, the cell membrane, that is impermeable to charged molecules except for the ion channels, acts as a capacitor and the membrane capacitance C can be defined as

$$C = \frac{Q}{V} , \tag{2.1}$$

where V is the membrane potential and Q is the excess negative charge on

the interior surface. Typically, membrane capacitances ranges from 0.1 to 1 nF. To define the membrane resistance let us consider a small constant current I_e injected into a neuron. This small current will cause the resting potential V to shift by an amount ΔV; then, according to Ohm's law, we can define the membrane resistance R as

$$R = \frac{\Delta V}{I_e} \ . \tag{2.2}$$

Typically, the membrane resistance ranges from 10 to 100 $M\Omega$. The time scale for variations in the membrane potential is given by the membrane time constant τ, defined as the product of the membrane capacitance and the membrane resistance: $\tau = RC$. The membrane time constant typically ranges fro 10 to 100 ms.

Ions cross the cell membrane through the ion channels mostly because of the potential difference and the concentration difference between the neuron and the extracellular medium. The potential difference results in electric forces that act on charged particles. For instance, when the membrane potential is negative, as it is most of the time, positive ions are attracted into the neuron and negative ions are attracted outside it. On the other hand, the concentration difference gives rise to the phenomenon of diffusion, that causes ions to move from regions of high concentration to regions of low concentration. For instance, K^+ ions are more concentrated inside the neurons, so they are attracted outside the cell membrane by diffusion.

An ion can also cross the cell membrane as a result of thermal fluctuations, since the thermal energy of ions and the membrane potential have the same order of magnitude. Let us consider, for instance, a positive ion with charge q inside a neuron with a negative membrane potential V. The electric field opposes the crossing of the cell membrane, but the ion can still leave the neuron if it has enough thermal energy to pass the potential barrier generated by the membrane potential. The minimum energy required to cross the barrier (i.e to leave the neuron) is $-qV$, which is positive since V is negative. The probability of finding an ion with thermal energy E is given by the Boltzmann distribution

$$P(E) = \frac{1}{k_B T} e^{-E/k_B T} \ , \tag{2.3}$$

where k_B is the Boltzmann constant and T is the temperature. The fraction of ions with enough energy to cross the barrier is then $\exp(qV/k_B T)$.

The diffusion current can be conveniently described introducing an equilibrium potential, that is defined as the membrane potential at which there is a balance between the diffusion current and the current due to potential difference. Let us consider the example of positive ions and a negative membrane potential V once again, and let us consider an ion channel that allows only a single type of ions to pass through. If the concentration of

such type of (positive) ions is higher inside the neuron, this might compensate for the action of electric forces. In fact, if we call [inside] and [outside], the concentrations of ions inside and outside the neuron, then the number of ions entering the neuron per second will be proportional to [outside] while the number of ions leaving the neuron per second will proportional to [inside] $\exp(qV/k_BT)$; the Boltzmann factor is due to the action of electric forces, that prevent ions that do not have enough thermal energy to overcame the potential barrier from leaving the neuron. The net current will be zero at the equilibrium potential V_{ep}, which gives the equation

$$[\text{outside}] = [\text{inside}]e^{qV_{ep}/k_BT} \ . \tag{2.4}$$

The solution is

$$V_{ep} = \frac{k_BT}{q} \ln\left(\frac{[\text{outside}]}{[\text{inside}]}\right) , \tag{2.5}$$

which is the Nernst equation. Ion channels relative to different types of ions can take very different values; for instance, K^+ channels have equilibrium potentials between -70 and $-90\ mV$, while Ca^{2+} channels have equilibrium potentials around $150\ mV$. As for channels that allow more than one type of ions to pass through, they are described in term of a reversal potential, which takes an intermediate value between the equilibrium potentials of the ions allowed to cross the channels.

Equation (2.4) shows that the current passing through an ion channel moves the membrane potential towards the equilibrium potential of that channel. Since the resting value of the membrane potential is around $-70\ V$, lower equilibrium potentials will make V more negative while higher equilibrium potential will make it less negative. The former process is called hyperpolarization, the latter is called depolarization. For instance, K^+ channels tend to hyperpolarize a neuron while Ca^{2+} tend to depolarize it.

The sum of all the currents flowing across all ion channels gives the total membrane current I_m. Such current is conventionally defined as positive when positive ions leave the neuron. For many ion channels the current is approximately proportional to $V - V_{ep}$. The proportional factor is defined as the inverse of the channel resistance. Summing over all types of channel gives the following expression for the total membrane current:

$$I_m = \sum_i \frac{1}{R_i}(V - V_{ep}^i), \tag{2.6}$$

where R_i is the resistance relative to channel i.

Ion channels behavior is affected by many factors, such as voltage variation or the concentration of some type of ions. As a consequence, channel resistances R_i change with time, making neuronal dynamics more complex. Nevertheless, some of the R_i, like the ones relative to ion pumps, are approximately constant and can be summed into a single term of the form

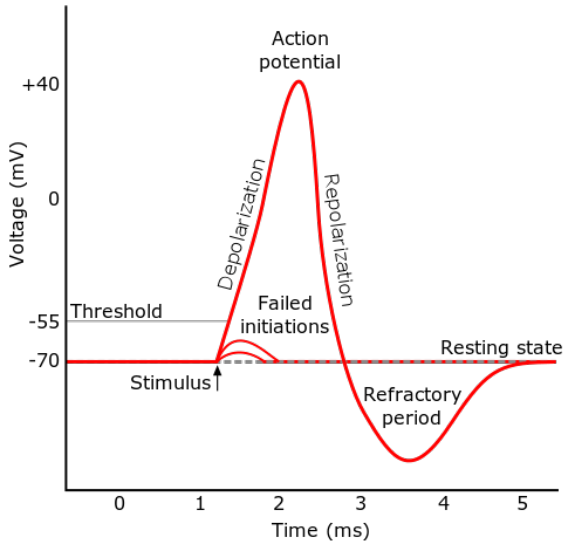

Figure 2.2: Drawing of a typical action potential. A stimulus gives rise to a fluctuation of the membrane potential of about 100 mV that lasts for about 1 ms. The action potential is followed by the refractory period, a time interval during which the neuron cannot fire new action potentials.

$\frac{1}{R_{eff}}(V - V_{eff})$, where R_{eff} and V_{eff} are the effective resistance and the effective equilibrium potential and do not depend on time. Such term is called leakage current.

2.1.2 Neuronal dynamics

Typically, an inactive neuron has a resting membrane potential $V_r \approx -70mV$. This is due mostly to the presence of open K^+ channels, that cause V to be close to the K^+ equilibrium potential. In fact, K^+ equilibrium potential ranges from -90 to -70 mV, which is very close to the typical resting membrane potential [26]. The membrane potential can be altered by the opening of channels relative to other types of ions. For instance, if the membrane potential reaches the value of about -45 mV, voltage dependent Na^+ channels open. Since the Na^+ equilibrium potential is around 50 mV, such opening will depolarize the neuron. After the depolarization the resting membrane potential is quickly restored by the closing of the Na^+ channels and the by the opening of K^+ channels.

The sequence of events just described gives rise to a fluctuation of the membrane potential of about 100 mV that lasts for about 1 ms (see figure 2.2). Such fluctuation is called action potential, and occurs only when the membrane potential crosses the threshold value for the opening of Na^+ channels. Action potentials are the only membrane potential fluctuations

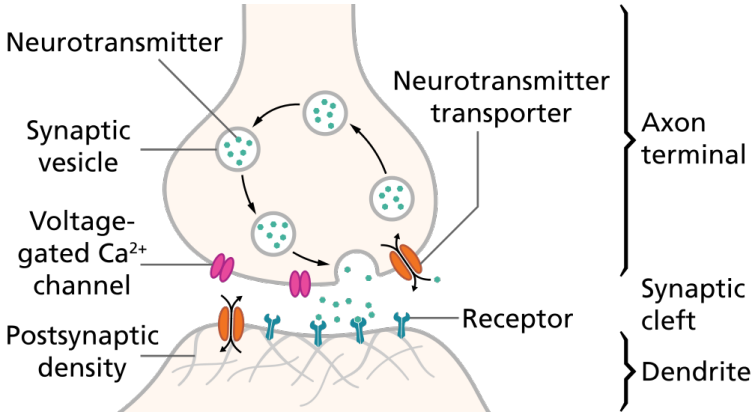

Figure 2.3: Drawing of a synapse. The synapse connects the axon of the presynaptic neuron to the dendrites of the postsynaptic neuron. On the presynaptic side, neurotransmitters are stored in synaptic vesicles. An action potential can cause a vesicle to release a neurotransmitter, which can bind to a receptor on the postsynaptic side.

that can travel over large distances. In fact, while fluctuations below the threshold weakens with increasing distance, action potentials are regenerated along axons so that they can reach synapses and carry information to other neurons.

Synapses usually connect the axon of a neuron to the dendrites of another neuron. When an action potential is fired, it travels along the axon until it reaches the synapses. Here, stored in small structures called synaptic vesicles, there are chemicals called neurotransmitters (see figure 2.3). The action potential may cause a vesicle to release a neurotransmitter that, in turn, can bind to a receptor on the receiving side of the synapses. This may cause a synaptic ion channel to open, causing, in turn, a variation in the membrane potential of the receiving neuron. Synapses that open channels that depolarize the neuron are called excitatory, while synapses that hyperpolarize the neuron are called inhibitory.

Before starting the description of neuron models, let us introduce two biological features that will be useful in the following: refractoriness and short-term synaptic depression. The former refers to the fact that, after a neuron has fired an action potential, it cannot fire again for a certain time interval, which is called refractory period. The latter refers to the fact that the probability of releasing a neurotransmitter can be affected by the past activity of the synapse. In particular, if a synaptic channel is activated twice in a small time interval, the current flowing through it after the second activation might be less than the current induced by the first activation; this feature is called short-term synaptic depression.

2.2 The integrate-and-fire model

In order find a relation between the fluctuations of the membrane potential and the membrane current let us go back to formula (2.1), which defines the membrane capacitance. Multiplying by V and taking the time derivative gives

$$C\frac{dV}{dt} = \frac{dQ}{dt} \ , \tag{2.7}$$

which states that the rate of change of the membrane potential and the rate at which charge builds up inside the neuron are proportional. But dQ/dt is also the total current I_{tot} that crosses the membrane potential. It will be convenient to write this current as the sum of two terms: the membrane current I_m, that is the total current passing through ion channels, and an external current I_e, that can be thought of as a current injected into the neuron through an electrode. Substituting into equation (2.7) gives

$$C\frac{dV}{dt} = -I_m + I_e \ , \tag{2.8}$$

where I_m has a negative sign because it is conventionally defined as positive when positive ions leave the neurone, while I_e is defined as positive when positive ions enter the neuron. The total membrane current can be thought of as the sum of a leakage current and more complicated time-dependent current terms, such as the ones relative to voltage dependent or synaptic channels.

In the previous sections we saw that when the membrane potential reaches the threshold for the opening of Na^+ channels an action potential is generated by the depolarizing action of Na^+ ions and the subsequent hyperpolarization due to K^+ ions. Furthermore, every time an action potential is fired, the membrane potential follows approximately the same trajectory. In the integrate and fire model the action of Na^+ and K^+ ions during the emission of an action potential is not reproduced. Instead, an action potential is registered every time the membrane potential reaches a threshold value V_{th}. After the emission the potential is simply reset to his rest value V_{rest}. In this way only the subthreshold fluctuations need to be modeled, which highly simplifies the task. In the simplest integrate-and-fire model, which is called leaky integrate-and-fire model, the membrane current I_e is given only by the leakage current, which gives the equation

$$C\frac{dV}{dt} = -\frac{V - V_{rest}}{R} + I_e \ . \tag{2.9}$$

The effective resistance in the leakage current term is precisely the membrane resistance R defined in formula (2.2), as can be checked by looking for the stationary solution of equation (2.9) in case of a constant I_e. Looking at equation (2.9) we can see that the neuron is modeled like an electrical circuit

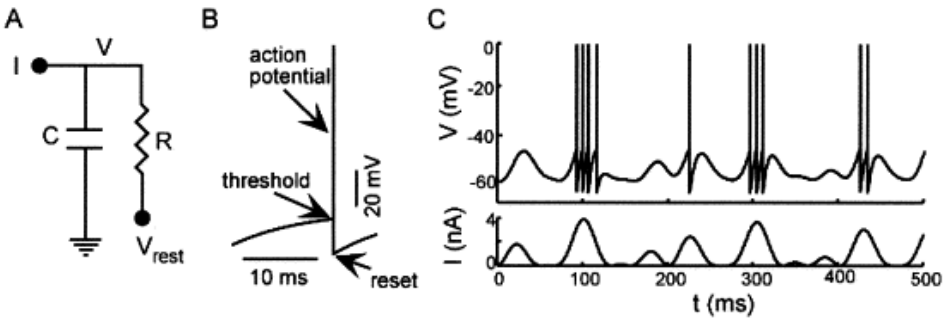

Figure 2.4: The integrate-and-fire model. A)The equivalent circuit. B)Membrane potential trajectory during an action potential; when the threshold has been reached, a spike is drawn and the potential is reset. C) Membrane potential variations under the injection of an external current I. Drawings from Abbott, 1999 [27].

with a resistance and a capacitor, as the one in figure 2.4: such circuit is called the equivalent circuit. In this model the action of synaptic ion channels is not reproduced.

The integrate-and-fire model was developed by Lapicque in 1907 [27]. At that time the biological mechanisms responsible for the generation of action potentials were not known and could not be included in the model. Nowadays such mechanisms are well understood and new models have been developed to represent them (see, for instance, Hodgkin and Huxley, 1952 [28]). Nevertheless, integrate and fire models are still widely used in the description of neurons. Of course, integrate-and-fire models of today are more complicated than the simple electrical circuit of the original Lapicque model; such models, for instance, can include synaptic currents. But even though the description of subthreshold fluctuations has become more accurate, the dynamics of spike potential emission is still not reproduced. This could be explained considering that there are two time scales at play: the scale of the slow subthreshold processes and the scale of the fast action potential emission. Since the fast action potential emission has a stereotypical character, sometimes it is useful to avoid the computational cost of calculating the membrane potential trajectory during such emission. Integrate-and-fire models reproduce only slow-scale processes, which is particularly useful for the description of large networks of neurons, that requires a big computational effort.

Chapter 3

Criticality in neural networks: the Millman Model

The experimental observation of self-organized criticality in cortical networks described in the first chapter has been confirmed also by theoretical models. In this chapter we describe a specific neuronal network model, the Millman Model. In particular, we show that not only does it predict the existence of neuronal avalanches whose size distribution obeys a power law, but also that such power law has an exponent of about $-3/2$, the same value observed by Beggs and Plenz.

3.1 Description

The Millman Model was developed by Millman, Mihalas, Kirkwood and Niebur in 2010 [29]. In the model a set of leaky integrate-and-fire neurons interact through excitatory synapses, so that when a neuron fires an action potential, a synaptic current can cause a depolarization of the membrane potentials of the neurons connected to it.

A network of N neurons is built in this way. Each neuron can receive synaptic inputs from, on average, other n_s neurons, that are extracted from the N neurons with uniform probability. The probability that a neuron will receive inputs from k other neurons is given by a Poisson distribution:

$$P(k) = \frac{(n_s)^k e^{-n_s}}{k!} \ . \tag{3.1}$$

It is important to remark that synapses are one-way connections. If, for instance, a neuron A is one of the neurons that can send synaptic inputs to neuron B, this means that there is a synapse that carries information from A to B and not backwards, so that neuron B cannot send synaptic inputs to A through that synapse.

The propagation of an action potential is modeled in this way. When a neuron fires a spike, this may or may not affect postsynaptic neurons. In fact, for each synapse, there are n_r synaptic vesicles that can release a neurotransmitter with probability p_r. If a neurotransmitter is released, the post-synaptic neuron receives a depolarizing synaptic current of the form

$$I_{in} = w_{in} e^{-(t-t_s)/\tau_s} \ , \tag{3.2}$$

where t_s is the time when the spike was fired. The model reproduces short-term synaptic depression scaling p_r by a time dependent factor

$$U(t) = 1 - e^{-(t-t_r)/\tau_R} \ , \tag{3.3}$$

where t_R is the time when the vesicle released the last neurotransmitter. In this way a vesicle that has just released a neurotransmitter has an almost zero probability of emitting another one; the probability then goes back to p_r with a characteristic time τ_R.

In addition to the synaptic inputs, neuron receive on average f_e external inputs per second with Poisson distribution, so that the probability that a neuron will receive k external inputs during a time interval Δt is

$$P(k) = \frac{(f_e \Delta t)^k e^{-f_e \Delta t}}{k!} \ . \tag{3.4}$$

The external input gives rise to a synaptic current of the form

$$I_e = w_e e^{-(t-t_s)/\tau_s} \ , \tag{3.5}$$

where t_s is the time of the external input.

The model reproduces also the refractory period; in fact, every time a neuron fires a spike, its potential is reset to the rest value V_r and does not change for a period τ_{rp}.

For a given neuron, the equation that describes the subthreshold dynamics of the membrane potential is then

$$C\frac{dV}{dt} = -\frac{V - V_r}{R} + \Big(\sum_i I_e^i(t) + \sum_j \sum_k H\big(p_r U_k(t_s^j) - \zeta\big) I_{in}^j(t) \Big) \ , \tag{3.6}$$

where H is the Heaviside function and ζ is a random variable with uniform distribution on $[0, 1]$. The first term on the right-hand side is just the leakage current while the second term contains the external and synaptic currents. Index i runs over the external inputs, index j runs over the action potentials fired by presynaptic neurons and index j runs over the synaptic vesicles that might have been affected by spike j.

3.2 Algorithms

Simulations of neural networks are commonly implemented by two classes of algorithms: synchronous or clock-driven algorithms and asynchronous or event-driven algorithms [34].

In synchronous algorithms there is a fixed time step Δt, and the state of each neuron is updated at every time step. Typically, during an iteration of a clock driven algorithm:

- incoming spikes (internal or external) are processed for each neuron;
- the membrane potential of each neuron is updated from t to $t + \Delta t$;
- membrane potentials that have crossed the threshold are reset to the resting value.

Asynchronous algorithms do not work with a fixed time step; instead, simulations evolve from an event to the next one, and only neurons that emit or receive action potentials are updated. Event driven algorithms work with a queue where events, such as the emission of a spike or the arrival of an external input, are stored. Typically, during an iteration of a clock driven algorithm:

- the event with the lowest timing is extracted from the queue;
- if the event is an external input, the state of the neuron that receive the input is updated to the time of the event; then, the time of the next spike of the neuron is calculated and stored in the queue;
- if the event is the emission of a spike, the state of the neuron that fires the spike is updated to the time of the event, its potential is reset and the time of the next spike of the neuron is calculated and stored in the queue; then, the state of the neurons that can receive the spike is updated to the time of the event, the changes due to the spike arrival (for instance, the generation of a synaptic current) are applied and the times of the next spikes are calculated and stored in the queue.

Synchronous algorithms are easier to implement than asynchronous ones, but less precise. In fact, the drawback of using a fixed time step is that spike times are bound to a discrete grid. Furthermore, since the value of membrane potentials are checked only at every Δt, some spike can go undetected. On the other hand, with asynchronous algorithms spike times are computed exactly; furthermore, such algorithms are more efficient since the state of each neuron is updated only when it receives an input and when it fires a spike, and not at every small step Δt. The drawback of event driven algorithms is that they are more difficult to implement than clock driven ones.

Table 3.1: Model parameters used in the simulations. The parameters are typical of cortical neurons (see, for instance, Dobrunz and Stevens, 1997[36]).

R $(G\Omega)$	C (pF)	V_r (mV)	V_{th} (mV)	w_e (pA)	f_e (Hz)	τ_s (ms)	τ_{rp} (ms)	τ_r (ms)	w_{in} (pA)
$\frac{2}{3}$	30	-70	-50	95	5	5	1	100	50

n_r	n_s	p_r
6	7.5	0.25

We have written two algorithms in order to make simulations of networks of neurons described by the Millman model: a clock driven algorithm and an event driven one. Both algorithms are able to reproduce the results obtained by Millman et al., as shown in the next paragraph. Nevertheless, the presence of both algorithms has been necessary for the analysis presented in the next chapter.

3.3 Numerical results

The properties of networks of neurons described by the Millman model have been investigated numerically using both the clock driven and the event driven algorithm. All simulations have been made using the parameters in table 3.1, which are typical of cortical neurons [35][36] and are the same parameters used by Millman et al. in their original paper [29].

3.3.1 Firing rate

The firing rate f is defined as the average number of spikes per neuron per second. It has been calculated averaging the number of action potentials during time intervals of 100 ms and normalizing. The analysis (see figure 3.1) shows that the networks alternate between two different states, characterized by two different levels of activity: an active state with high spiking activity ($f \approx 60$ spikes s^{-1}) and a quiescent state with low spiking activity ($f \approx 0$ spikes s^{-1}). The active state is called up state and the quiescent state is called down state.

The fluctuations between up and down states that emerge from the simulations have been observed experimentally in networks of cortical neurons (see, for instance, Plenz and Kitai, 1998) [37]. It is important to remark that such fluctuations are a network phenomenon; in fact, they occur because a large number of neurons simultaneously alternate between a quiescent state

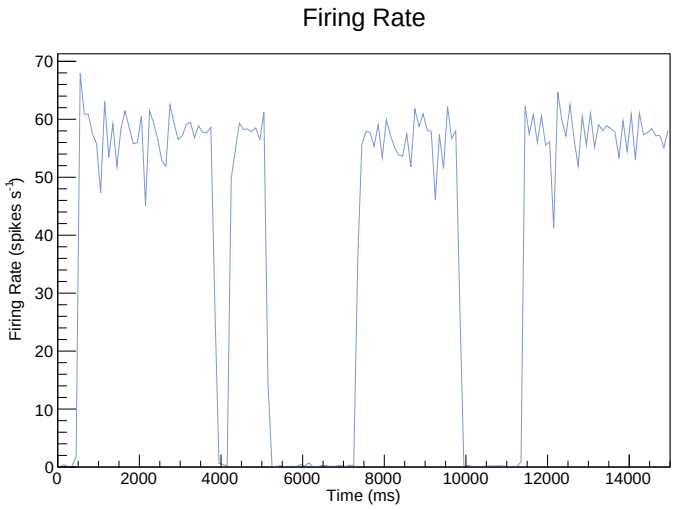

Figure 3.1: Firing rate for a network of 300 neurons. The network alternates between up states ($f \approx 60$ spikes s^{-1}) and down states ($f \approx 0$ spikes s^{-1}). Model parameters as in table 3.1.

and an active state, as it has been shown experimentally [38] and by numerical simulations [29].

3.3.2 Up/down state duration

The durations of up and down states have been studied simulating the networks for 15000 s and averaging over ten different simulations. The analysis shows that the up state duration distribution is fitted by an exponential distribution, as shown in figure (3.2), in agreement with other simulations [29].

The up state duration has been studied for networks of different sizes and the analysis shows that the duration distributions of such networks have different characteristic times. In order to further investigate this aspect, networks of seven different sizes (from 200 to 800 neurons) have been simulated. For each size the mean and the variance of the duration histograms have been calculated and averaged over ten different simulations. The results are shown in figure 3.3, where the characteristic times relative to different sizes have have been plotted in lin-log coordinates. The plot shows that the logarithm of the characteristic time grows approximately linearly with the size of the system, so that the characteristic time τ can be approximated as an exponential function of the size s:

$$\tau(s) \approx e^{s/s_{up}} \ ,$$

with $s_{up} \approx 110$.

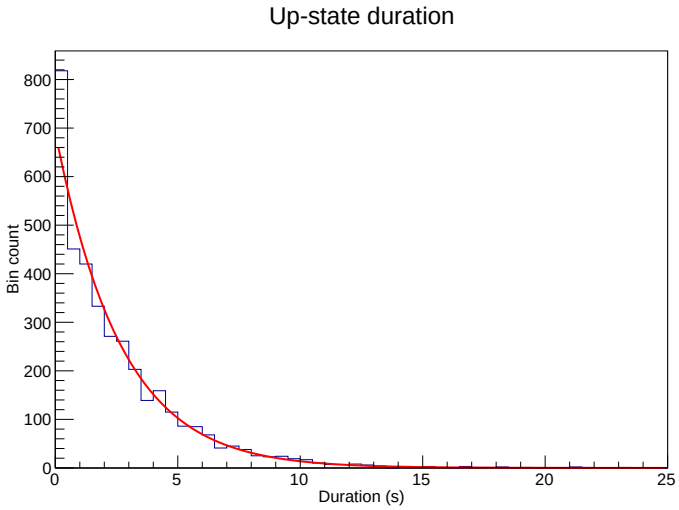

Figure 3.2: Up state duration for a network of 300 neurons. The histogram is fitted by an exponential distribution with characteristic time $\tau \approx 2.5\ s$. Model parameters as in table 3.1.

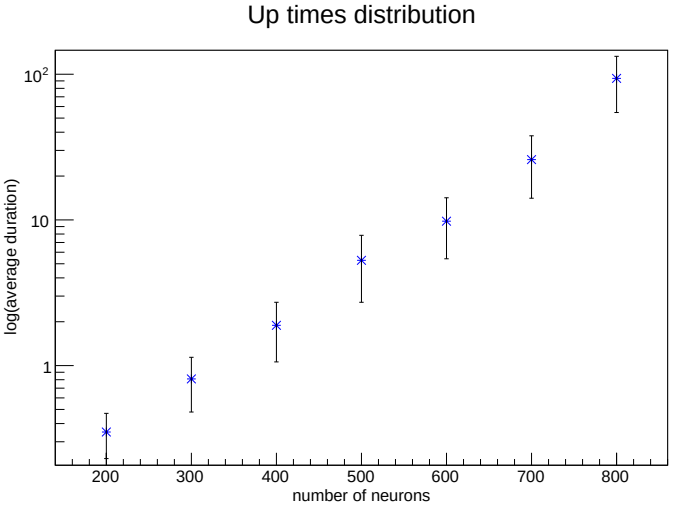

Figure 3.3: Plot of the characteristic time of up states for networks of different size. The characteristic time grows with the size of the network. The plot is in lin-log coordinates. Model parameters as in table 3.1.

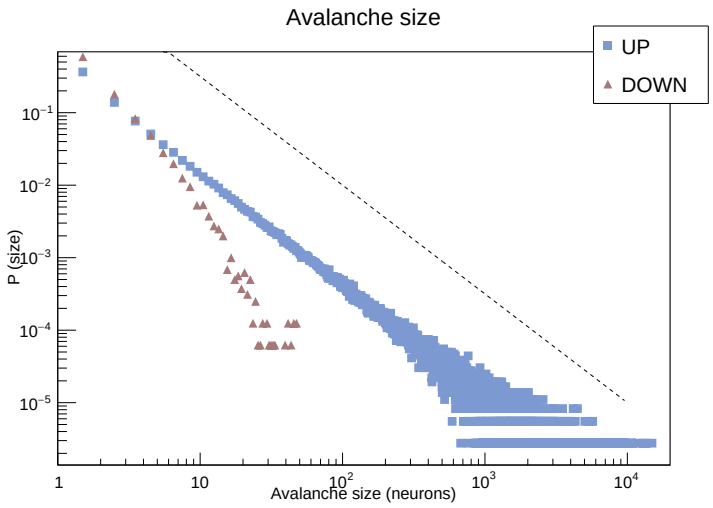

Figure 3.4: Avalanche size distribution for up (in blue) and down (in brown) states in log-log coordinates. The dashed line corresponds to a power law with slope $-3/2$. Simulations on networks of 2500 neurons, model parameters as in table 3.1.

The same analysis has been performed on down states duration. As for up states, the characteristic time of down states can be approximated as an exponential function of the size, with $s_{down} \approx 730$ (results not shown).

3.3.3 Avalanches

When an action potential is fired, it propagates to postsynaptic neurons and can result in a depolarization of their membrane potentials. If a postsynaptic neuron is sufficiently depolarized, the action potential can cause it to fire too, and so on. This chain of events describes a neuronal avalanche.

In the Millman model avalanches are defined in this way: an avalanche starts when an external input cause a neuron to fire an action potential; when a neuron fires as a consequence of an internal input, the neuron is considered a member of the same avalanche of the presynaptic neuron. Neuronal avalanches have been analyzed separately for up and down states. For each of the two states, the size and the lifetime distributions have been studied, as shown in figure (3.4) and (3.5). The distributions have been obtained using simulations of networks with 2 500 neurons. A total of 378 011 avalanches have been analyzed, 361 967 in the up state and 16 044 in the down state. The activity of the network has been simulated for 150 s, during which the system has been in the up state for 102 s and in the down state for the remaining 48 s. This gives an average of 3 545 avalanches per second in the up state and 335 in the down state.

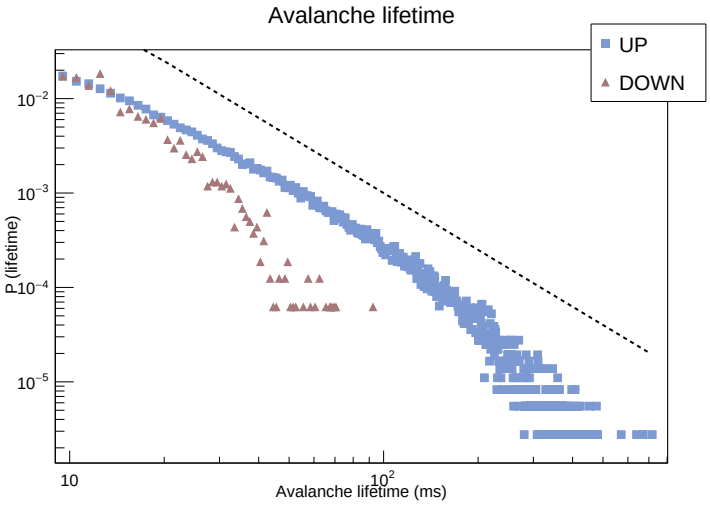

Figure 3.5: Avalanche lifetime distribution for up (in blue) and down (in brown) states in log-log coordinates. The dashed line corresponds to a power law with slope -2. Simulations on networks of 2500 neurons, model parameters as in table 3.1.

The up state size distribution, as shown in figure (3.4), exhibits a power law behavior. The exponent has been found to be

$$\alpha = -1.57 \pm 0.01, \tag{3.7}$$

not far from the exponent $-3/2$, corresponding to the dotted line in figure (3.4). The up state lifetime distribution exhibits a power law behavior in the central part of the plot and an exponential cutoff in the final part (the exponential cutoff in the lifetime distribution was observed also by Beggs and Plenz). The exponent has been found to be

$$\alpha = -1.91 \pm 0.02 \ , \tag{3.8}$$

not far from the exponent -2, corresponding to the dotted line in figure (3.5).

The observed power law behavior of up states is in agreement with the experimental analysis performed by Beggs and Plenz. Furthermore, the exponents observed in the distributions are close to $-3/2$ and -2, which are the same exponents observed by Beggs and Plenz and the same predicted by the theory for a critical branching process.

Figures (3.4) and (3.5) show that down state distributions behave differently from up state ones; in fact, the size distribution follow approximately a power law behavior only for small avalanches ($\lesssim$10), while the lifetime distribution do not exhibit a power law behavior at all.

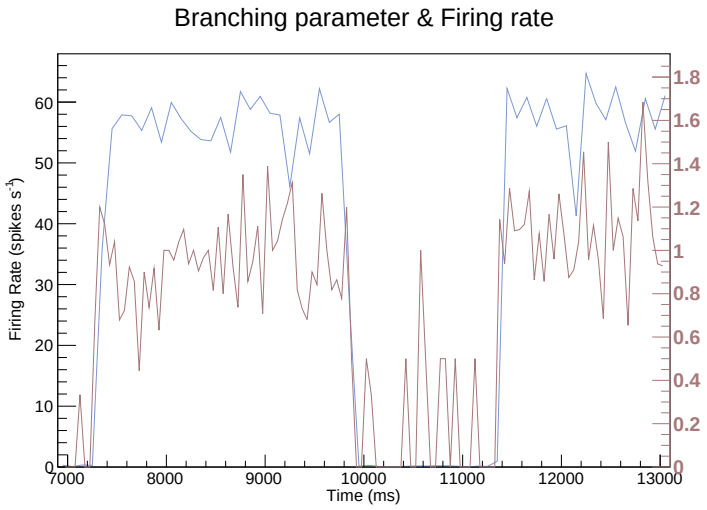

Figure 3.6: Plots of the branching parameter (in brown) and the firing rate (in blue) as functions of time. The values of the branching parameter are given by the axis on the right. During up states the branching parameter fluctuates around 1, during down states it fluctuates around 0.

3.3.4 Branching parameter

The branching parameter is defined as the average number of neurons that emit an action potential as a consequence of the synaptic input received from the first neuron of an avalanche. If we classify the neurons of an avalanche by generations, so that the neuron that initiates the avalanche belongs to first generation, the neurons activated by the first generation neuron belong to the second generation and so on, we can define the branching parameter as the average number of second generation neurons.

The branching parameter has been calculated as a function of time in order to study its behavior during up and down states. The results are shown in figure (3.6), where the branching parameter and the firing rate are plotted together. The analysis shows that during up states the branching parameter fluctuates around 1, while during down states it fluctuates around zero. This suggests that up states are critical while down states are not, as it is confirmed also by the observation that only up states exhibit power law (critical) behavior in size and lifetime distributions.

3.3.5 Spectrum

In order to study the spontaneous oscillations of the network, the power spectrum of the firing rate has been analyzed. Three types of power spectra have been computed: the spectrum of up and down states together and the spectra of up and down states alone. The latter have been calculated

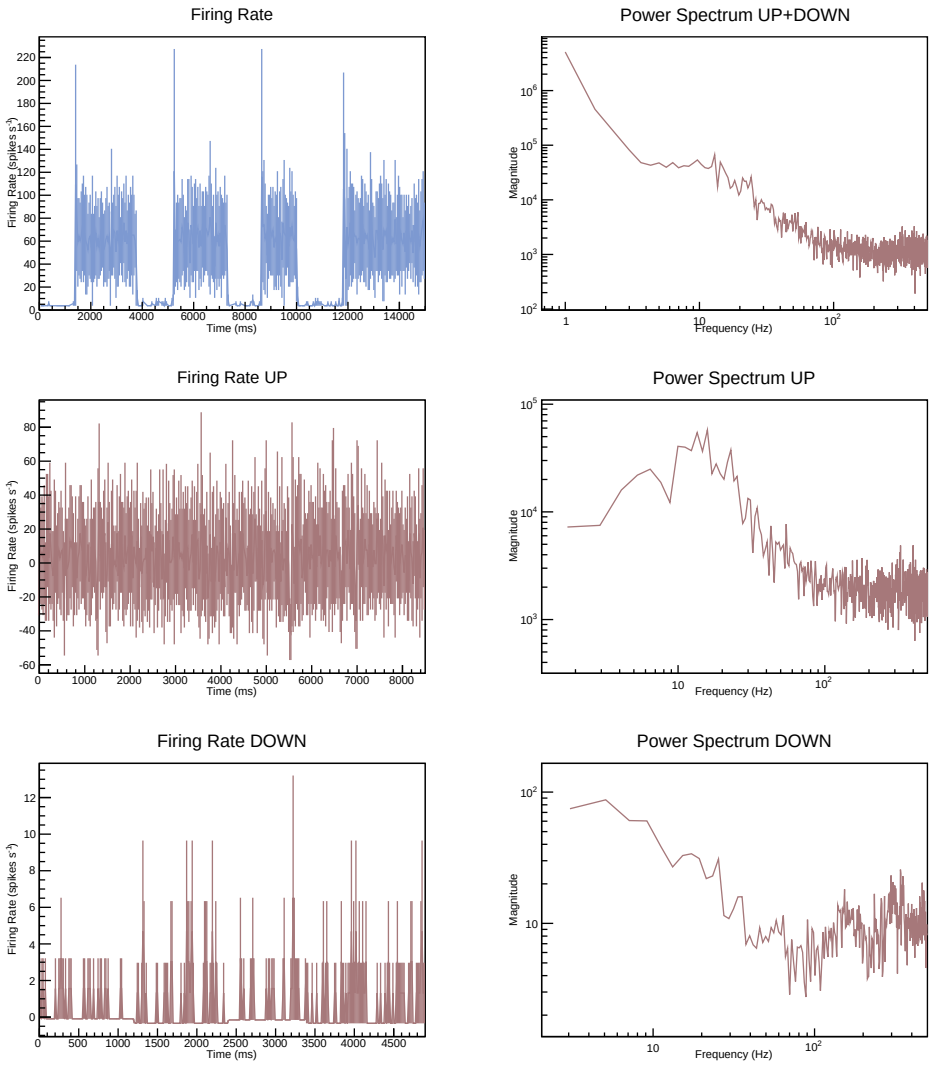

Figure 3.7: First column: firing rate for up and down states, only for up states, only for down states; in the second and third plots the mean value has been subtracted. Second column: power spectrum, in log-log coordinates, of the graphs in the first column. The spectrum of up and down states together exhibits a high spectral power in the 0.5-2 Hz band, due to the slow alternation between up and down states; the up state power spectrum shows a peak around 20 Hz.

putting together all up (resp. down) states of the simulation and subtracting the mean value. The results are shown in figure 3.7, where the power spectra have been plotted in log-log coordinates.

The spectrum of up and down states together exhibits a high spectral power in the 0.5-2 Hz band, due to the slow alternation between up and down states. This low frequency behavior vanishes in power spectra of up and down states alone. Furthermore, the up state power spectrum shows a peak around 20 Hz, which is not visible in the down state power spectrum. The presence of such peak has been observed both experimentally [39] and by means of theoretical models [40]. It has been suggested [41] that the peak is due to a mechanism called "Stochastic amplification of fluctuations" which gives rise to a resonant amplification of a band of frequencies of the spectrum. In short, this mechanism acts only on states that, at a deterministic level, can be described by attractors with complex eigenvalues of its Jacobian matrix [41]. Since only up states can be described in this way, this explains why the peak is not visible in the down state spectrum.

3.4 Analytical description

The critical properties of the network can also be studied analytically. Before dealing with the analysis of the Millman model, we briefly review some general methods by which integrate-and-fire models are studied analytically.

3.4.1 Fokker-Planck formalism

Let us consider a general integrate-and-fire model whose dynamics is given by equation

$$\tau \frac{dV}{dt} = -(V - V_r) + RI(t) \ , \tag{3.9}$$

where V_r is the resting potential and $RI(t)$ is the synaptic current. We assume [31][32] that each neuron receives a large number of inputs per integration time τ and that each of these inputs results in a small variation of V compared to the firing threshold; furthermore we assume that couples of neurons have a small number of common inputs. Under these assumptions the synaptic current $RI(t)$ in equation (3.9) can be approximated by an average part plus a fluctuating Gaussian part

$$RI(t) = (\mu(t) - V_r) + \sigma(t)\sqrt{2\tau}\xi(t) \ , \tag{3.10}$$

where $\xi(t)$ is a Gaussian white noise (see Appendix for the derivation). Furthermore the spike emissions of all neurons can be approximated by Poisson processes with a common instantaneous firing rate but otherwise uncorrelated. This means that, given the instantaneous firing rate $f(t)$, each neuron has a probability $f(t)dt$ of emitting an action potential between t and $t+dt$, but spike emissions are statistically independent in different neurons.

Substituting equation (3.10) in equation (3.9) gives:

$$\tau \frac{dV}{dt} = -(V - \mu(t)) + \sigma(t)\sqrt{2\tau}\xi(t) \ . \tag{3.11}$$

Equation (3.11) can be transformed [31][30] into a Fokker-Planck equation describing the evolution of the probability distribution of membrane potentials

$$\tau \frac{\partial P(V,t)}{\partial t} = \frac{\partial}{\partial V}\Big(\big(V - \mu(t)\big)P(V,t)\Big) + \sigma^2(t)\frac{\partial^2 P(V,t)}{\partial V^2} \ . \tag{3.12}$$

The Fokker-Planck equation is equivalent to the following set of equations

$$\begin{cases} \dfrac{\partial P(V,t)}{\partial t} = -\dfrac{\partial J(V,t)}{\partial V} \\ J(V,t) = -\dfrac{1}{\tau}\big(V - \mu(t)\big)P(V,t) - \dfrac{\sigma^2(t)}{\tau}\dfrac{\partial P(V,t)}{\partial V} \end{cases} , \tag{3.13}$$

where $J(V,t)$ is the probability current passing through V at time t.

3.4.2 Firing rate

The firing rate $f(t)$ is defined as the average number of action potentials per second per neuron at time t and is given by the flux through the threshold $J(V_{th},t)$. Equation (3.13) shows that, in order for f to be finite, $P(V,t)$ has to be continuous in V_{th}. Therefore, since $P(V,t) = 0$ for $V > V_{th}$ because the potential of an integrate-and-fire neuron cannot be above the threshold, we must impose the boundary condition $P(V_{th},t) = 0$. Substituting in equation (3.13) then gives:

$$f(t) = -\frac{\sigma^2}{\tau}\frac{\partial P(V_{th},t)}{\partial V} \ . \tag{3.14}$$

Since membrane potentials that cross the threshold are reset to the resting potential V_r, and since after the reset they remain inactive for a refractory period τ_{rp}, there is an additional probability current through V_r at time $t + \tau_{rp}$ which is equal to the current through the threshold at time t [32].

The Fokker-Planck formalism derived here is extremely useful for investigating the dynamics of networks of spiking neurons, and can be extended to include networks with synaptic input described by an inhomogeneous Poisson process (that is, by a Poisson process with a time dependent Poisson parameter $\lambda(t)$), that gives rise to time dependent $\mu(t)$ and $\sigma(t)$ in equation (3.12). The Millman model describes one of these networks.

3.4.3 Fokker-Planck equation for the Millman model

In order to write down the Fokker-Planck equation for the Millman model we need to approximate the synaptic current on the right-hand side of equation (3.6) by an average part plus a Gaussian part, as it was done in equation (8). That is, we need to write

$$R\sum_i I_e^i(t) + R\sum_j\sum_k H\big(p_r U_k(t_s^j - \zeta) I_{in}^j(t)\big) = (\mu(t) - V_r) + \sigma(t)\sqrt{2\tau}\xi(t) \ , \tag{3.15}$$

where $\mu(t)$ and $\sigma(t)$ are the time dependent mean and variance we need to determine. It can be shown (see Appendix for the derivation) that the time dependent $\mu(t)$ and $\sigma(t)$ are given by

$$\begin{cases} \mu(t) = V_r + \tau V_{in} u n_s f(t) + \tau V_e f_e \\ \sigma^2(t) = \dfrac{\tau (V_{in} u)^2 n_s f(t)}{2} + \dfrac{\tau V_e^2 f_e}{2} \end{cases} . \tag{3.16}$$

where $V_{in} \equiv w_{in}\tau_s p_r n_r / C$ and $V_e \equiv w_e \tau_s / C$ are the mean changes in the membrane potential due to a single internal or external input. Substituting in equation (3.12) we obtain the Fokker-Planck equation for the Millman model.

3.4.4 Branching parameter

Let us consider a neuron that receives a synaptic input from another neuron in the network. As we saw in the previous sections, on average such an input will cause the membrane potential to change by an amount uV_{in}. The neuron will then fire an action potential only if its membrane potential is closer to the threshold than uV_{in}. The probability that this happens times the average number of connections per neuron gives the branching parameter σ:

$$\sigma = n_s \int_{V_{th} - uV_{in}}^{V_{th}} dV P(V, \infty) \ , \tag{3.17}$$

where we have used the long time limit (stationary) probability distribution. Since an individual input causes a little change in the membrane potential compared to the threshold (that is, $uV_{in} \ll V_{th} - V_r$), the integral can be approximated by the slope near threshold, giving

$$\sigma \approx -\frac{n_s (uV_{in})^2}{2} \frac{\partial P(V_{th}, \infty)}{\partial V} \ . \tag{3.18}$$

It can be shown [29] (see Appendix for the derivation) that, at stable states, σ is given by

$$\sigma = \frac{n_s V_i n^2 f^*}{V_e^2 f_e (1 + p_r \tau_r f^*)^2 + n_s V_{in}^2 f^*} \ , \tag{3.19}$$

where f^* is the firing rate at stable states.

3.4.5 Analytical results

The dynamics of the network was studied by Millman et al. [29]. They used the Fokker-Planck equation to evolve an initial probability distribution into stationary states. By means of the time derivatives of u (see Appendix for an analytical calculation) and f,that was obtained numerically, they studied the fixed point of the dynamics using different values of the parameters.

Figure 3.8 shows the values of the firing rate and of the branching ratio at the fixed points for different values of two of the parameters of the model: the amplitude of the internal synaptic current w_{in} and the characteristic recovery time of synaptic vesicles τ_R. We can see that, when the synapses are sufficiently strong and the vesicles recover quickly enough, the system has two stable fixed points: an active state characterized by a high firing rate and a branching parameter close to one, and a quiescent state, with f and σ both approaching zero. Knowing that, at fixed points, the mean synaptic utility can be written as (see Appendix for the derivation)

$$u^* = \frac{1}{1 + p_r \tau_R f^*} \ ,$$

we see that during the active states u^* is small (neurotransmitters are released with high frequency), while it approaches to one during the quiescent states, when the vesicles have the time to recover before the arrival of the next spike.

Lowering w_{in} and increasing τ_R (that is, taking networks with weaker synapses and longer recovery times) leads to networks with unstable active states, while networks with very low w_{in} e very large τ_R have only the quiescent state.

These results are in agreement with numerical simulations. In fact, if we pick parameter values typical of cortical neurons [33], both numerical simulation and analytical calculations show that the networks are characterized by two different states: up states and down states. Up states are active states with high firing rate and branching parameter approaching to one and down states are quiescent states with low firing rate and branching parameter approaching to zero. The value of the branching parameter of the two states can be obtained numerically and analytically. The results are the same for both calculations and show that the up state is critical ($\sigma \approx 1$) and the down state is subcritical ($\sigma \approx 0$).

3.5 Conclusions

The analysis of the Millman model described in this chapter shows that, during the up state, the network exhibits the features of a self-organized critical system. In fact, neuronal activity is characterized by avalanches whose size and lifetime distributions follow a power law, the branching parameter is

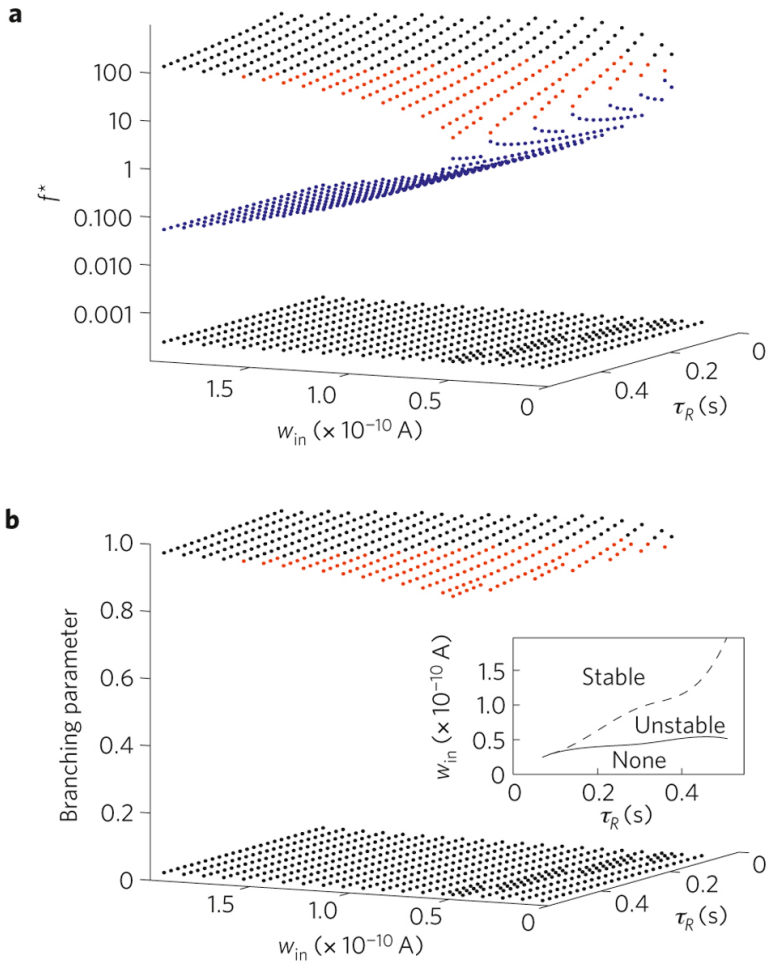

Figure 3.8: a) The firing rate at the fixed points for different values of w_{in} and τ_R. Stable fixed points are drawn in black, unstable fixed points in red and saddle nodes in blue. b) The branching parameter at the fixed points for different values of w_{in} and τ_R. Plots from Millman et al., 2010 [29].

close to one, and criticality is robust to variations of the parameters (there is no need for external tuning) [29].

Even though these features have also been observed by Beggs and Plenz in their experimental analysis of cortical neurons, there are many differences between the way these results have been obtained experimentally and the way they have been obtained by theoretical models. The analysis of these differences will be performed in the next chapter.

Chapter 4

Beggs and Plenz's analysis on the Millman model - The direct method

In the first chapter we saw how neuronal avalanches were experimentally observed in networks of cortical neurons by Beggs and Plenz. The size and lifetime distributions of these avalanches are described a power law, which is a signature of criticality. Another signature of criticality is the fact that the exponents of the power law distributions are the same predicted by the theory for a critical branching process, 3/2 and 2. Furthermore, the branching parameter has been shown to be close to the critical value $\sigma = 1$.

In the third chapter we studied the theoretical predictions of a leaky integrate and fire neuron model, the Millman model. We saw that the model predicts, numerically and analytically, the existence of two different network states: an active state, called up state, and a quiescent state, called down state. We saw that the up state is characterized by power law distributions of size and lifetime with exponents close to 3/2 and 2 and by a branching parameter close to one, the same behavior observed by Beggs and Plenz in networks of cortical neurons.

The analogies between experimental observations and theoretical predictions support the idea that cortical neurons are self-organized critical systems that work at the boundary between a runaway activation of the network and a state where neural activity quickly decreases over successive steps; furthermore, they suggest that neuronal activity occurs in avalanches whose dynamics can, to some extent, be reproduced by the Millman model. However, despite the analogies, the way avalanches are defined and detected in the experimental analysis is very different from the way they are defined and detected in theoretical simulations.

In the following chapters we investigate the differences between theoretical and experimental avalanches; in particular, we analyze the data from

numerical simulations with the experimental methods used by Beggs and Plenz to detect avalanches in networks of cortical neurons. We show that, if the methods of analysis change, the results are completely different.

4.1 Theoretical versus experimental avalanches

In the Millman model by definition an avalanche starts when an external input causes a neuron to fire an action potential. If the action potential causes other neurons to emit a spike, these neurons are considered members of the avalanche, and so on. Therefore, if we want to detect the avalanches, it is not enough that we know the timings of the spikes; we need to know also what causes each neuron to fire a spike, if it is an external input, in which case we register the beginning of an avalanche, or an internal one, and if it is an internal one we need to know where does it come from, so that we can include the neuron in the avalanche of the presynaptic neuron. Luckily, in theoretical simulations we can get all the information we need just by modifying the algorithms, so that avalanches can be easily detected.

The situation is completely different when avalanches have to be detected experimentally (see table 4.1). This time we do not have access to all the information, but only to a fraction of it. We do not know, for instance, what type of input makes a neuron fire, nor where does such an input come from. In fact, we are not even able to detect individual spikes, but only extracellular voltage variations (LFPs) in the vicinity of each electrode, as we saw in the first chapter. Because of this lack of information, avalanches have to be defined differently in experimental networks. We saw that Beggs and Plenz set a threshold and associated an event to each LFPs that crossed the threshold. Then, they binned the data and counted the events in each bin. An avalanche was then defined as a sequence of successive bins with at least one event between two bins with no events.

Since, despite the different definitions of neuronal avalanche, both the theoretical and the experimental analysis showed the same power law behavior of size and lifetime distributions, one might wonder what would happen if theoretical data were to be analyzed as if they were experimental ones. Would the power law behavior still be observed in theoretical simulations if avalanches were to be defined as in Beggs and Plenz analysis? In the rest of the chapter we try to answer this question using three different methods.

4.2 Direct method

The first method consists in treating the spike times given by theoretical simulations as if they were the events of the experimental analysis. The membrane potential of each neuron of the theoretical network is analyzed as if it were the signal from an electrode, and each spike is treated as an

Theoretical avalanches	Experimental avalanches
An avalanche starts when an external input causes a neuron to fire an action potential.	An avalanche starts when there is a bin with at least one event after a bin with no events.
Neurons that fire after being excited by members of an avalanche become members of the same avalanche.	Events in a bin that follows a non empty bin become members of the same avalanche.
An avalanche ends when none of its members causes other neurons to fire.	An avalanche ends when an empty bin occurs.

Table 4.1: Differences between theoretical and experimental avalanches.

LFP. A theoretical network of N neurons is therefore analyzed as a cultured slice on a N-electrode array. Furthermore, the information taken from the theoretical data is only the spike times, all the rest is ignored in order to simulate the lack of information of the experimental analysis. We call this method of analysis the direct method.

4.2.1 Interevent interval and branching parameter

In the first chapter we saw that, in order to detect avalanches, it was necessary to choose a time interval Δt to bin the data. We also saw that Beggs and Plenz suggested that the correct interval to be used was the interevent interval, which they defined as the average time interval between consecutive events during an active period. Following this line of reasoning, in the following analysis the interevent interval (IEI) has been defined as the average time interval between consecutive action potentials.

Beggs and Plenz defined the branching parameter in two different ways in their work: as the average number of events in the second bin of an avalanche initiated by a single event, and as the ratio of the events in the first bin of an avalanche to the events in the second bin. In order to average over the maximum possible number of avalanches, in the following analysis the second definition of branching parameter has been used.

In the previous chapters we saw that in theoretical simulations the branching parameter is defined as the as the average number of second generation neurons, while in experimental analysis it is defined as in Beggs and Plenz's work. In order to distinguish between the two branching parameters, from now on the former will be called σ and the latter σ_{bp}.

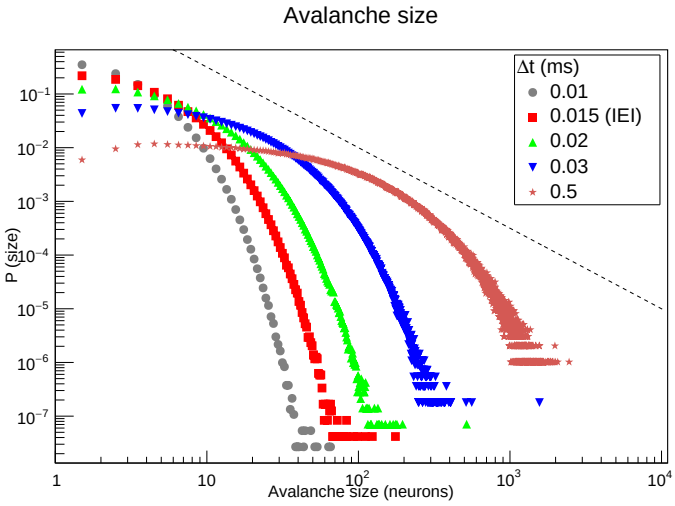

Figure 4.1: Up-down state. Plots of avalanche size distribution calculated using five different time intervals to bin the data. The distributions do not follow the expected power law with exponent $-3/2$ (dashed line) as in Beggs and Plenz's analysis [13]. Simulations of networks of 1200 neurons.

4.2.2 Up-down state

The direct method has been used in two different ways: first, it has been applied to up and down states together (we refer to this as up-down state), then it has been applied separately to each of them. In both cases the analysis has been performed using several simulations of networks of different sizes, giving similar results. In the next paragraphs we discuss the results given by two of these simulation, one for up and down states together and one for up and down states alone. Let us start with the first one.

The data from a $1.5 \cdot 10^4$ seconds simulation of a network of 1200 neurons have been binned using five different time intervals, one of them being the IEI; then, for each value of the bin interval, the size and lifetime distributions have been calculated. The analysis, see figures 4.1 and 4.2, shows that, no matter what the bin interval is, neither the size distribution nor the lifetime distribution follow a power law anymore.

The total number of avalanches calculated using the direct method has been compared to the total number of avalanches calculated with the method of the third chapter. The former will be called n_{exp} and the latter n_{th}. If we analyze the network using all the information at our disposal, we find $n_{th} \approx 25 \cdot 10^6$ avalanches. If, on the other hand, we analyze the system with Beggs and Plenz's method, the number of avalanches n_{exp} depends on the binning time, ranging from about a million to almost 40 millions. Remarkably, the binning time that gives the number closest to n_{th} is the

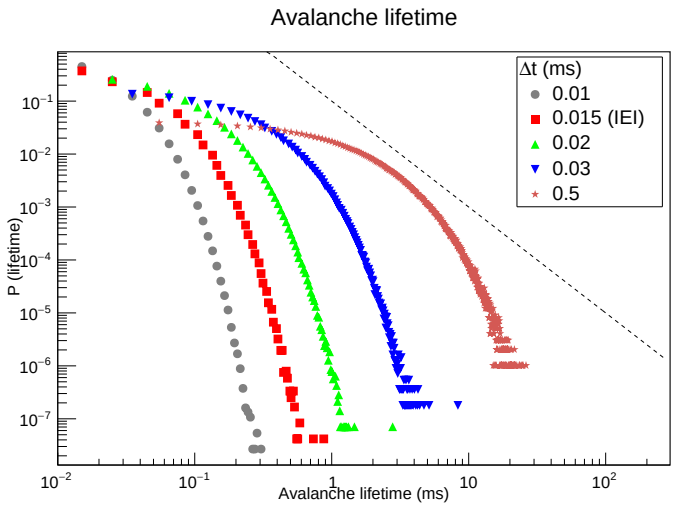

Figure 4.2: Up-down state. Plots of avalanche lifetime distribution calculated using five different time intervals to bin the data. The distributions do not follow the expected power law with exponent -2 (dashed line) as in Beggs and Plenz's analysis [13]. Simulations of networks of 1200 neurons.

IEI, which gives $n_{exp} \approx 24 \cdot 10^6$ avalanches.

4.2.3 Up state analysis and down state analysis

The analysis performed in the previous chapter showed that networks of neurons described by the Millman model alternates between an active state, called up state, characterized by high spiking activity, and a quiescent state, characterized by an almost zero firing rate. This suggests that the methods of analysis described in the previous section could be applied separately to up and down states. In order to do this, two different time intervals have been used: one for the binning of up state data and one for the binning of down state data.

Up state

A $1.5 \cdot 10^4$ seconds simulation of a network of 300 neuron has been analyzed separately for up and down states. The analysis of up states has given results very similar to those of the previous section, where up and down states have been studied together. In fact, as can be seen in figures 4.3 and 4.4, size and lifetime distributions do not follow a power law.

The comparison between n_{th} and n_{exp} has given results different from the analysis of up-down state. In fact, n_{th} has been found to be around $3.2 \cdot 10^6$ avalanches, while n_{exp}, with the IEI as binning time, has been found to be

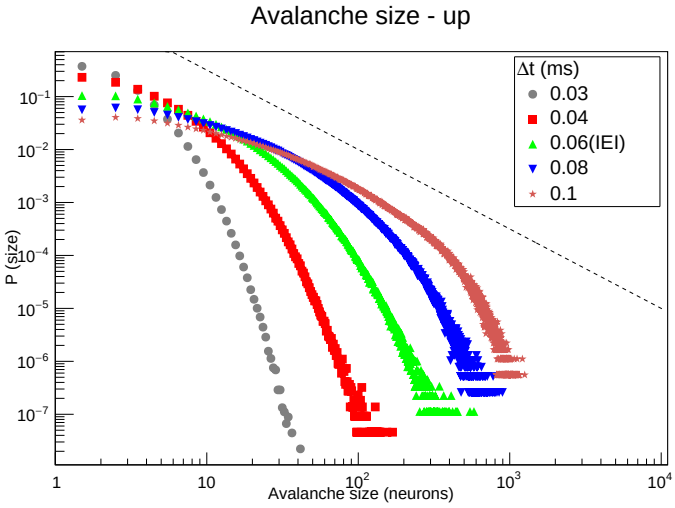

Figure 4.3: Avalanche size distribution relative to up states, calculated using five different time intervals to bin the data. The distributions do not follow the expected power law with exponent $-3/2$ (dashed line) as in Beggs and Plenz's analysis [13]. Simulations of networks of 300 neurons.

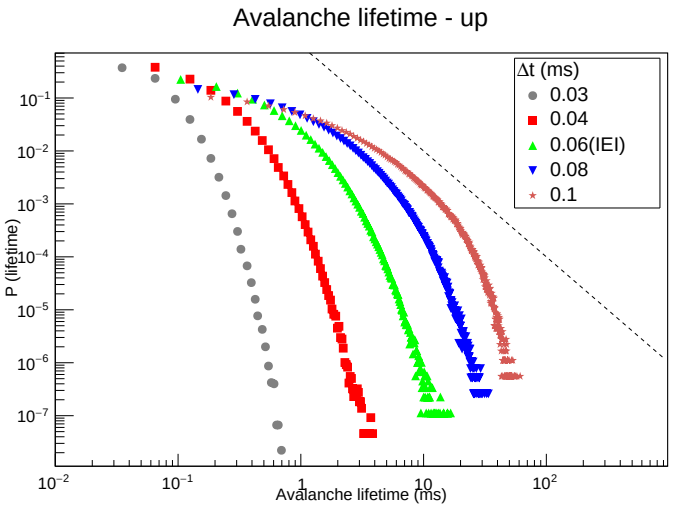

Figure 4.4: Avalanche lifetime distribution relative to up states, calculated using five different time intervals to bin the data. The distributions do not follow the expected power law with exponent -2 (dashed line) as in Beggs and Plenz's analysis [13]. Simulations of networks of 300 neurons.

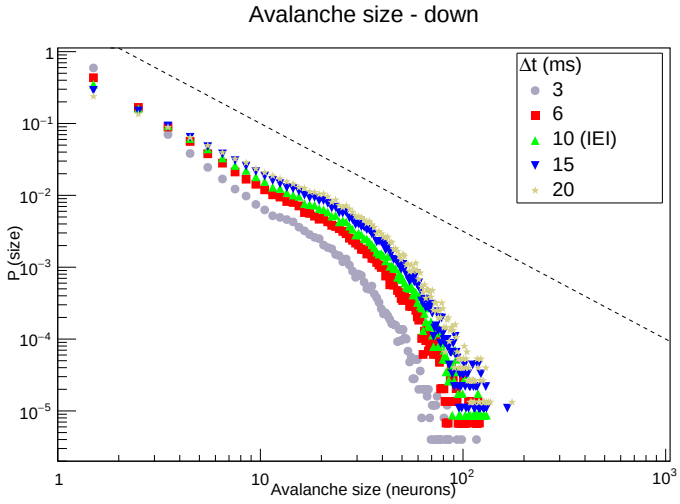

Figure 4.5: Avalanche size distribution relative to down states, calculated using five different time intervals to bin the data. The distributions follow a power law for sizes $\lesssim 10$. The dashed line corresponds to a power law with exponent $-3/2$. Simulations of networks of 300 neurons.

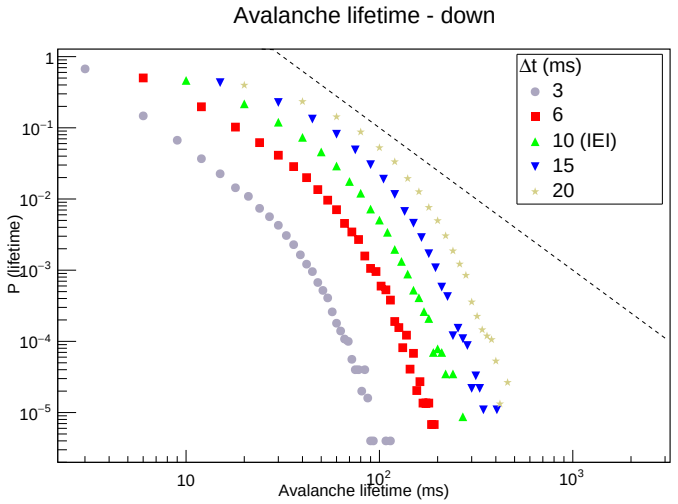

Figure 4.6: Avalanche lifetime distribution relative to down states, calculated using five different time intervals to bin the data. The distributions do not follow a power law, except for the one relative to $\Delta t = 3$ ms, which exhibits power law behavior for sizes $\lesssim 20$. The dashed line corresponds to a power law with exponent -2. Simulations of networks of 300 neurons.

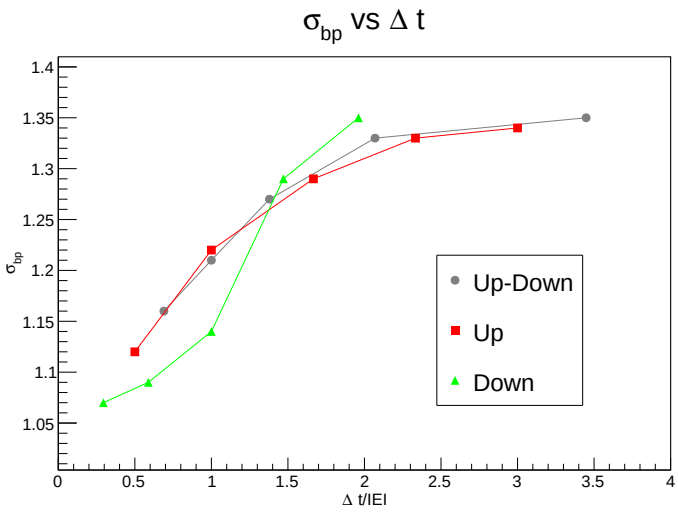

Figure 4.7: Branching parameter σ_{bp} as a function of the binning interval. The value of σ_{bp} increases with increasing binning interval. The x axis gives the binning interval as a multiple of the IEI.

approximately $21 \cdot 10^6$ avalanches. We see that, contrary to what has been found in the previous section, the two numbers are not close.

Down state

Things change when the down state is analyzed. In fact, the size distribution, as can be seen in figure 4.5, shows approximately a power law behavior for sizes $\lesssim 10$. The initial slope is dependent on the binning time, and the slope relative to the IEI is around the critical value $-3/2$. On the contrary, the lifetimes distributions do not show a power law behavior, except for the one relative to the smaller time bin, which exhibits power law behavior for sizes $\lesssim 20$. Curiously enough, the initial slope of such distribution is not far from the critical value -2.

The comparison between n_{th} and n_{exp} has given $n_{th} \approx 3 \cdot 10^5$ avalanches and $n_{exp} \approx 10^5$ avalanches. As usual, n_{exp} has been calculated using the IEI as binning time.

4.2.4 Branching parameter

The branching parameter σ_{bp} has been calculated for each choice of the binning interval Δt. The analysis, as can be seen in figure 4.7, shows that σ_{bp} depends on the binning interval and, in particular, it shows that over the range under examination σ_{bp} increases with increasing Δt. The branching parameter relative to up and up-down state has been found to be $\sigma_{bp} \approx 1.2$, when it was measured taking the IEI as bin size; instead, the branching

parameter of down states has been found to be $\sigma_{bp} \approx 1.15$. Such values are far from the critical value $\sigma_{bp} = 1$, which was measured by Beggs and Plenz in networks of cortical neurons.

4.2.5 Conclusions

The analysis described in the previous paragraphs shows that, when theoretical data are analyzed using the direct method, the size and lifetime distributions of up-down state and of up state do not show a power law behavior. Down states size distributions, on the contrary, have been found to follow a power law for small sizes ($\lesssim 10$). This is in agreement with the results of chapter 3 (see figure 3.4), which show that, when avalanches are detected using all the information available, down state size distribution follows approximately a power law for sizes $\lesssim 10$, while down state lifetime distribution does not. The power law behavior exhibited by down state distributions is unexpected and needs further investigation since, according to theoretical predictions (see section 3.4.5), down states are not critical.

The fact that down state distributions agree with the results of chapter 3, whereas up and up-down distributions do not, can be explained in this way. Since down state is characterized by low spiking activity, usually avalanches last for a short time and are separated by pauses that are longer then the avalanches lifetimes. When this happens, theoretical and experimental avalanches coincide for a wide range of bin sizes[1]. The fact that some of the bin sizes we used are out of such a range, and the fact that sometimes different avalanches occur at the same time give rise to some differences between the theoretical and the experimental analysis, and explain the dependence of the slope in figure 4.5 on the bin size.

During up states avalanches mix, meet, split and are not separated by long pauses; in this situation, experimental avalanches are completely different from theoretical ones, as can be seen comparing figure 3.4 with figure 4.3.

The analysis performed in this chapter also shows that the branching parameter depends on the binning time and that, when it is calculated using the IEI to bin data, it is far from the critical value $\sigma_{bp} = 1$, which was measured by Beggs and Plenz in networks of cortical neurons.

[1] In order for this to happen the bin size has to remain bigger than the minimum distance between consecutive events in the same burst of activity and shorter than the pauses between consecutive bursts.

Chapter 5

Beggs and Plenz's analysis on the Millman model - The subset method

The direct method, described in the previous chapter, consists in analyzing each spike as if it were an LFP. One of the objections that could be raised to this method is that in real experiments only a fraction of the network can be monitored. In the experiment described in the first chapter, for instance, a brain slice was put on a multielectrode array, where the distance between each electrode and its nearest neighbor was 200 μm. Since the signal at each electrode was due to synchronized action potential emission from the neurons in the vicinity of the electrode [15][16][17], only the slice areas close to the electrodes were monitored during the experiment.

In order to simulate this further lack of information, the spike times of different subsets of the neurons in a network have been extracted from the data; then, the analysis of the previous section has been performed only on these spike times. This method of analysis will be called the subset method.

As the direct method, the subset method has been applied to up and down states together (we refer to this as up-down state) and to each of them alone. The analysis has been performed on data from simulations of networks of different sizes, with similar results. In the next paragraphs we discuss the results given by two of these simulations.

5.1 Up-down state

Subsets of 100, 225, 300 and 450 neurons have been randomly extracted from a network of 900 neurons. The spike times of the neurons in each subset have been extracted from the data of a 1500 seconds simulation and have been analyzed with the subset method. The IEI has been calculated for each subset and such an interval has been used to bin the data, then the

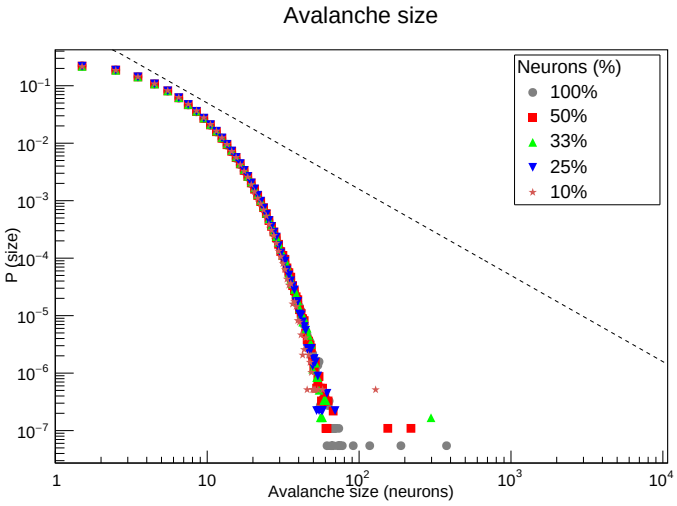

Figure 5.1: Plots of avalanche size distribution calculated using five different subsets of neurons. The distributions do not follow the expected power law with exponent $-3/2$ (dashed line) as in Beggs and Plenz's analysis [13]. Simulations of networks of 900 neurons.

avalanche size and lifetime distributions have been calculated.

Figures 5.1 and 5.2 show that neither the size nor the lifetime distribution follow a power law behavior, no matter what the fraction of neurons used in the analysis is. Figure 5.1 shows also that the size distributions of all the subsets collapse into a unique function. This is very different from what happened when Beggs and Plenz analyzed the system using the signal from different subsets of the electrodes. In that case, as we saw in the first chapter (see figure 1.4), each distribution had a cutoff around the number of electrodes used in the analysis, which means that most of the time an electrode was activated only once during an avalanche. Avalanches with size bigger than the number of electrodes were observed, but such events were very rare. On the contrary, using the subset method we have found that size distributions relative to different subsets collapse into a unique function, which suggests that many neurons contribute more than once to a single avalanche. Figure 5.2 shows that lifetime distributions relative to different subsets have the same shape.

In order to study the dependence of the distributions on the time interval used in the binning, the size and lifetime distributions of the 300 neurons subset have been calculated using five different time bins. The results, see figure 5.3 and 5.4, show that the distributions behave approximately as the ones calculated using the direct method. The branching parameter, as can be seen in figure 5.9, increases with increasing binning interval, as it has been found using the direct method.

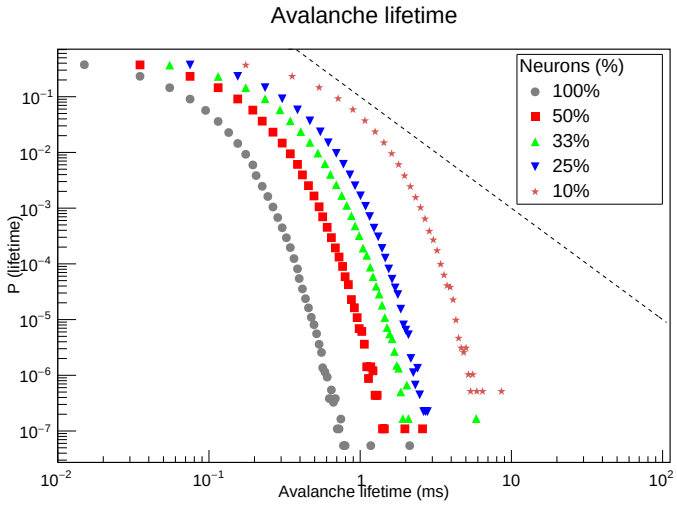

Figure 5.2: Plots of avalanche size distribution calculated using five different subsets of neurons. The distributions do not follow the expected power law with exponent -2 (dashed line) as in Beggs and Plenz's analysis [13]. Simulations of networks of 900 neurons.

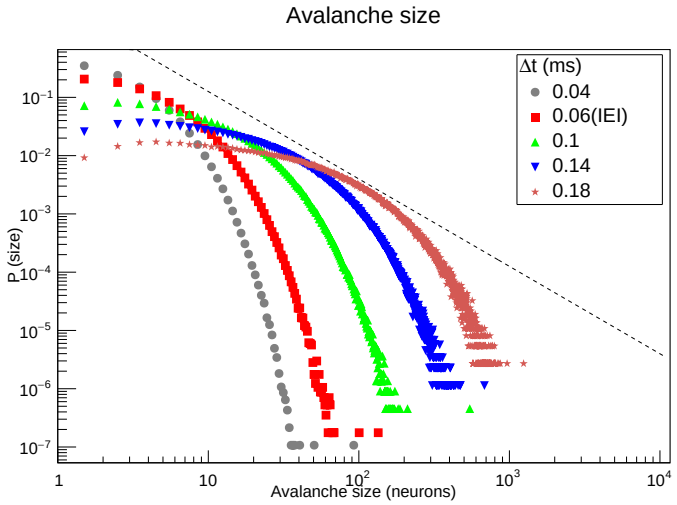

Figure 5.3: Up-down state. Plots of avalanche size distribution calculated using five different time intervals to bin the data. The distributions do not follow the expected power law with exponent $-3/2$ (dashed line) as in Beggs and Plenz's analysis [13]. Simulations of networks of 900 neurons, subsets of 300 neurons.

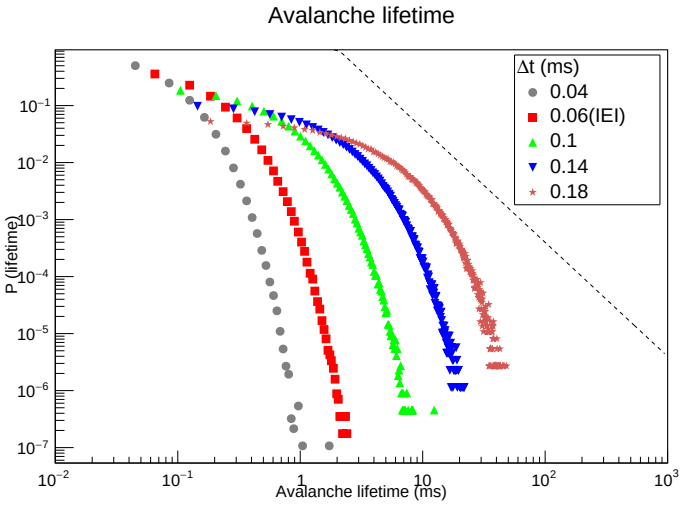

Figure 5.4: Up-down state. Plots of avalanche lifetime distribution calculated using five different time intervals to bin the data. The distributions do not follow the expected power law with exponent -2 (dashed line) as in Beggs and Plenz's analysis [13]. Simulations of networks of 300 neurons, subsets of 300 neurons.

5.2 Up state

The same analysis of the previous paragraph has been performed separately for up and down states, this time randomly extracting subsets of 50, 100, 150 and 200 neurons from a network of 300 neurons. We have simulated a network smaller than the one simulated for up-down state because, as can be seen in figure 3.3, the average duration of up (and down) states grows exponentially with the size of the network. As a consequence, a simulation of a bigger network migh have been dominated by one long up (resp. down) state, resulting a bad statistics for down (resp. up) state. The spike times of the neurons in each subset have been extracted from the data from a 1500 seconds simulation and have been analyzed with the subset method. For each subset the IEI has been calculated separately for up and down states and has been used to bin the data. Then, the avalanche size and lifetime distributions have been calculated.

Figure 5.5 and 5.6, show that, as for up-down state, the size and the lifetime distributions of up states do not follow a power law. The size distributions of all the subsets collapse into a unique function, showing that many neurons contribute more than once to a single avalanche. Also, lifetime distributions relative to different subsets exhibit the same shape.

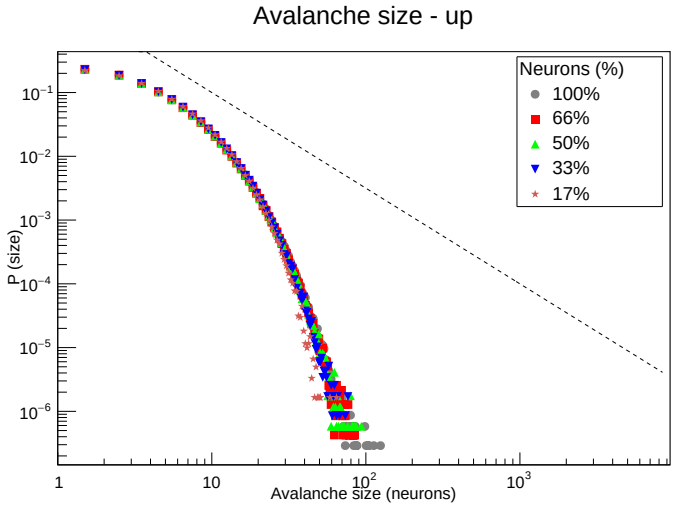

Figure 5.5: Up state. Plots of avalanche size distribution calculated using five different subsets of neurons. The distributions do not follow the expected power law with exponent $-3/2$ (dashed line) as in Beggs and Plenz's analysis [13]. Simulations of networks of 300 neurons.

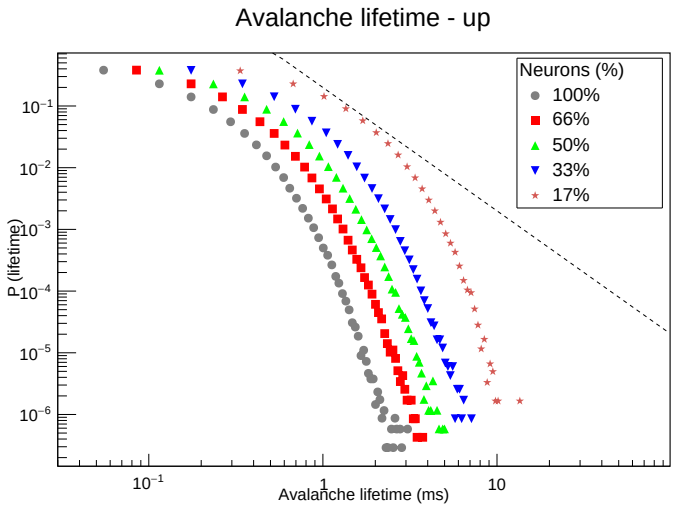

Figure 5.6: Up state. Plots of avalanche lifetime distribution calculated using five different subsets of neurons. The distributions do not follow the expected power law with exponent -2 (dashed line) as in Beggs and Plenz's analysis [13]. Simulations of networks of 300 neurons.

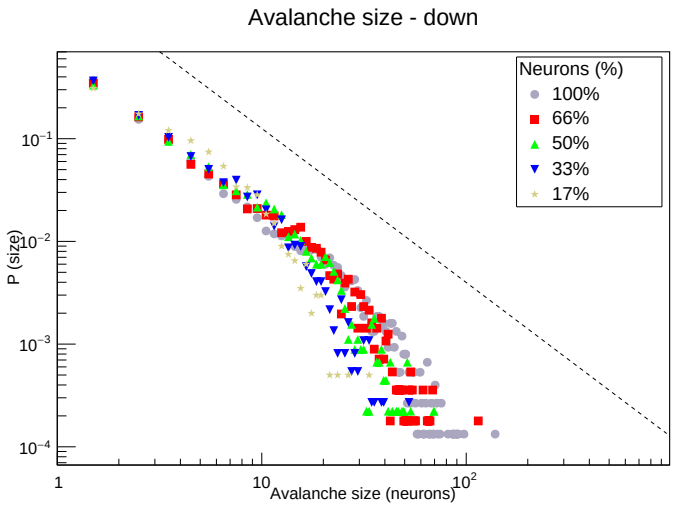

Figure 5.7: Down state. Plots of avalanche size distribution calculated using five different subsets of neurons. The distributions follow a power law for sizes $\lesssim 10$. The dashed line corresponds to a power law with exponent $-3/2$. Simulations of networks of 300 neurons.

5.3 Down state

The analysis of the down state has been performed on the same dataset used in the up state analysis. The plot of the size distributions (see figure 5.7) shows the same behavior already shown using the direct method: for sizes $\lesssim 10$ the distributions follow a power law behavior with slope approximately $-3/2$. As in the up state analysis, lifetime distributions relative to different subsets have the same shape.

5.4 Branching parameter

The branching parameter has been measured for each subset of neurons. In the case of up and up-down state, the fact that only a fraction of the system was analyzed did not affect the measure, as can be seen in figure 5.9. In fact, taking the IEI as bin size, the branching parameter has been found to be $\sigma_{br} \approx 1.2$ for each subset of neurons. This value, which is approximately the same value found with the direct method, is far from the critical value $\sigma_{bp} = 1$ measured by Beggs and Plenz. On the contrary, the branching parameter of down states changes with the fraction of neurons in the subset; in particular, it increases with decreasing subset size. However, for each subset it remains greater than the critical value.

The branching parameter has also been measured as a function of the bin size for a subset of 300 neurons in the up-down state; the results, as

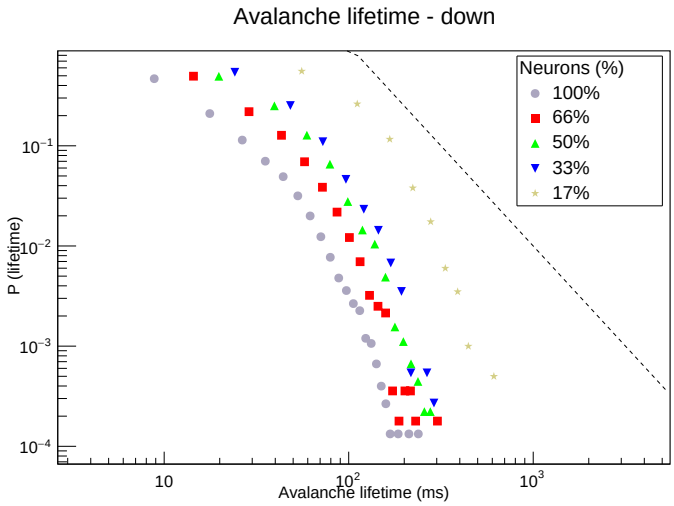

Figure 5.8: Down state. Plots of avalanche size distribution calculated using five different subsets of neurons. The distributions do not follow the expected power law with exponent -2 (dashed line) as in Beggs and Plenz's analysis [13]. Simulations of networks of 300 neurons.

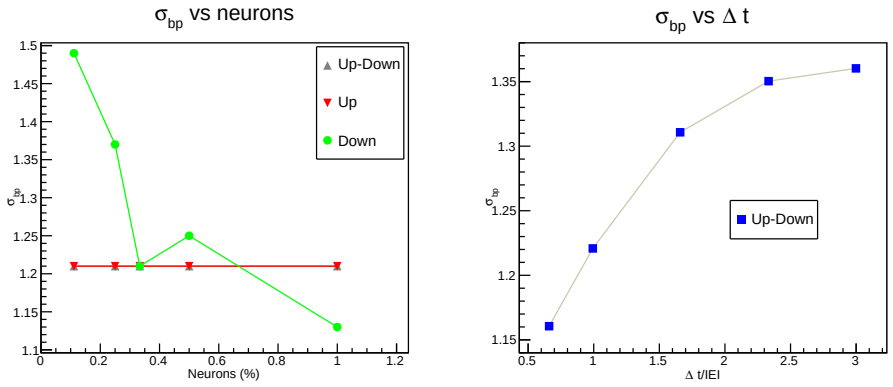

Figure 5.9: Left: σ_{bp} as a function of the fraction of neurons; σ_{bp} is constant for up and up-down states and is bigger for smaller subsets for down states. IEI taken as bin size. Right: σ_{bp} as a function of the binning interval for a subset of neurons in up-down state; σ_{bp} increases with increasing binning interval, as when the whole system is analyzed; the x axis gives the binning interval as a multiple of the IEI. Simulations of networks of 900 neurons, subsets of 300 neurons.

can be seen in figure 5.9, are very similar to those found using the direct method: σ_{bp} is an increasing function of the bin size and, when the IEI is set as binning interval, it has been found to be $\sigma_{br} \approx 1.2$, far from the critical value $\sigma_{bp} = 1$.

5.5 Conclusions

The results reported above show that performing the analysis on a subset of the data does not change the behavior of the distributions. In fact, the results are almost the same as the ones given by the direct method: the size and lifetime distributions of up and down states together and of up states alone do not follow a power law; on the contrary, the size distributions of down states follow a power law with exponent $-3/2$ for sizes $\lesssim 10$.

The branching parameter relative to up and up-down states has been found to be independent on the subset size, while the branching parameter relative to down states has been found to increase with decreasing subset size; however, when the IEI was set as bin size, σ_{bp} has always been found to be far from the critical value $\sigma_{bp} = 1$ measured by Beggs and Plenz.

The analysis shows also that typically a neuron contributes more than once to a single avalanche, while in Beggs and Plenz analysis usually an electrode was activated only once during an avalanche.

Chapter 6

Beggs and Plenz's analysis on the Millman model - The clustering method

Both the direct method and the subset method consist in treating action potentials as LFPs. One of the objections that could be raised to this approach is that an LFP is not caused by a single neuron, but depends on the activity of many neurons in the vicinity of the electrode [15][16][17]. The emission of a single spike in not enough to induce an LFP, many neurons have to fire synchronized action potentials in order for this to happen.

In order to simulate in a more realistic way the experimental method of analysis, the neurons of the network have been divided into clusters and a potential has been associated to each cluster. Such a potential has been defined as the sum of the membrane potentials of the neurons in the cluster. The clock driven algorithm has then been modified in order to give as output the value of each cluster potential at every time step of temporal evolution. Finally, the data have been analyzed treating each cluster potential as if it were the signal at an electrode; as in Beggs and Plenz analysis, a threshold has been set and an event (LFP) has been associated to each signal above the threshold. The events have then been analyzed as in the experimental analysis. We refer to this method of analysis as the clustering method.

The clustering method has been studied using only the clock driven algorithm because all cluster potentials had to be updated regularly, which is not guaranteed by the event driven algorithm.

6.1 Threshold

In the first chapter we saw that that Beggs and Plenz fixed the threshold value comparing the data to the noise, represented by a Gaussian distribution. This method could not be used in our analysis, since the signal at an

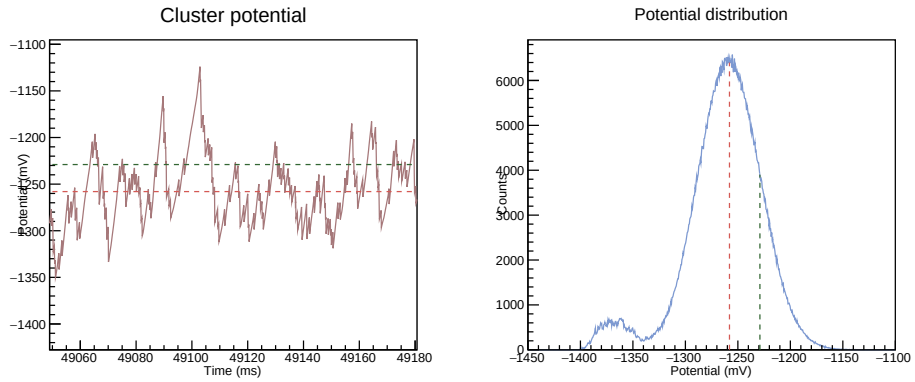

Figure 6.1: Left: cluster potential as a function of time; the dotted line represents the threshold value given by the mean plus the standard deviation of the up state peak. Right: cluster potential distribution; the peak on the left corresponds to down states, the one on the right corresponds to up states. Simulations on a network of 2000 neurons, clusters of 20 neurons.

electrode is very different from the signal given by a cluster potential. This can be seen comparing figure 1.1, where a typical action potential is plotted, and figure 6.1, where a typical cluster potential is shown.

An action potential has a stereotypical shape: a sharp negative peak that quickly relaxes to a rest value. On the contrary, a cluster potential has neither a stereotypical shape nor a rest value; instead, it seems to fluctuate irregularly around an average value. This can be seen looking at the potential distribution in figure 6.1. The distribution has two peaks: the one on the left corresponds to down states, where membrane potentials are more polarized (i.e. more negative), the one on the right corresponds to up states, where membrane potentials are, on average, depolarized. The difference in the peak heights shows that, during the simulation, the network has spent more time in the up state than in the down state. The shape of the distribution suggests that the mean of the Gaussian distribution that fits the up state peak could be chosen as the threshold value. Another possibility could be to choose the mean value plus the standard deviation. The clustering method has been tested using both thresholds, with similar results.

Once a threshold has been set, the analysis has been performed following Beggs and Plenz's procedure: for each excursion above the threshold, the maximum amplitude and the corresponding time have been calculated; the data have then been binned and avalanches have been defined and studied in the usual way.

Figure 6.1 shows that in the clustering method avalanches can be detected only in up states. In fact, during down states, the cluster potentials fluctuate around the mean value of the peak on the left, that is $\approx$ -1375 mV, far below

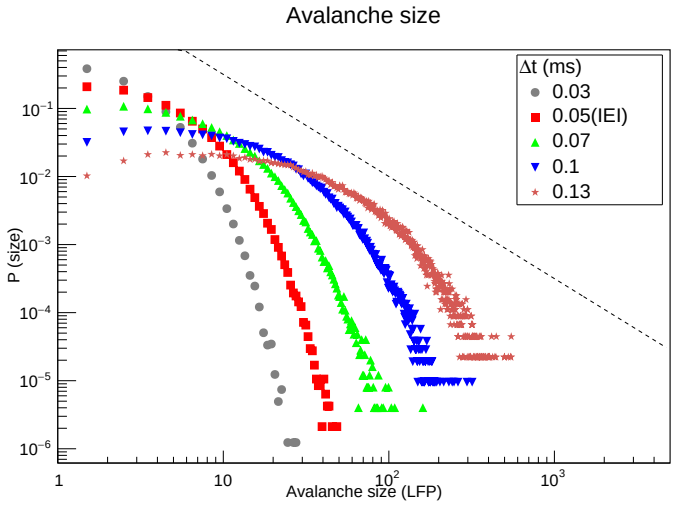

Figure 6.2: Plots of avalanche size distribution calculated using five different time intervals to bin the data. The distributions do not follow the expected power law with exponent $-3/2$ (dashed line) as in Beggs and Plenz's analysis [13]. Simulations of networks of 2000 neurons, clusters of 20 neurons.

the threshold values given both by the mean and by the mean plus the standard deviation of the peak on the right. The fact that the peaks are only slightly superimposed makes it very unlikely that an event could be registered during a down state.

6.2 Results

The clustering method has been applied to networks of different sizes and to clusters composed of different fractions of the neurons in the network, with similar results. In the following paragraphs we describe the analysis of a network of 2000 neurons. The data have been extracted from a 100 seconds simulation.

6.2.1 Analysis of all the clusters

The network of 2000 neurons has been divided into 100 clusters of 20 neurons. The data relative to cluster potentials have been extracted from the 100 seconds simulation of the network. The threshold has been defined as the mean plus the standard deviation of the up state peak. The processes data have been binned using five time intervals, one of them being the IEI. For each interval the size and lifetime distributions have then been calculated.

Figures 6.2 and 6.3 show that the distributions are very similar to those found using the direct (see figures 4.1 and 4.2) and the subset (5.3 and 5.4)

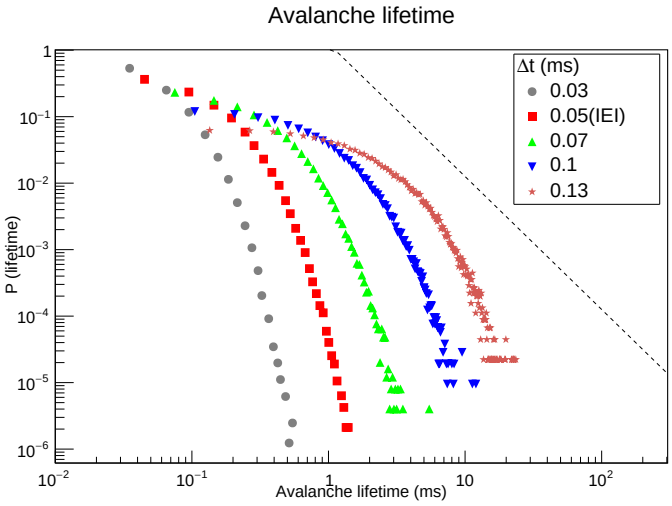

Figure 6.3: Plots of avalanche lifetime distribution calculated using five different time intervals to bin the data. The distributions do not follow the expected power law with exponent -2 (dashed line) as in Beggs and Plenz's analysis [13]. Simulations of networks of 2000 neurons, clusters of 20 neurons.

methods. In fact, neither the size nor the lifetime distributions follow a power law for any value of the bin interval.

6.2.2 Analysis of subsets of the clusters

In order to simulate the fact that in real experiments only a fraction of the network can be monitored, the data relative to three different subsets of the clusters have been extracted, as it was done in the subset method. The subset were composed of 25, 50 and 75 randomly chosen clusters. For each subset, the size and lifetime distributions have been calculated using the corresponding IEIs to bin the data. Figures 6.4 and 6.5 show that the distributions are very similar to those found using the subset method (see figures 5.1 and 5.2). The distributions do not follow a power law, no matter what the size of the subset of clusters is. The size distributions relative to different subsets collapse into a unique function, showing that a cluster usually contributes with more than one event to a single avalanche, contrary to what happens when real data are analyzed (see chapter one). Figure 6.5 shows that lifetimes distributions relative to different subset have the same shape.

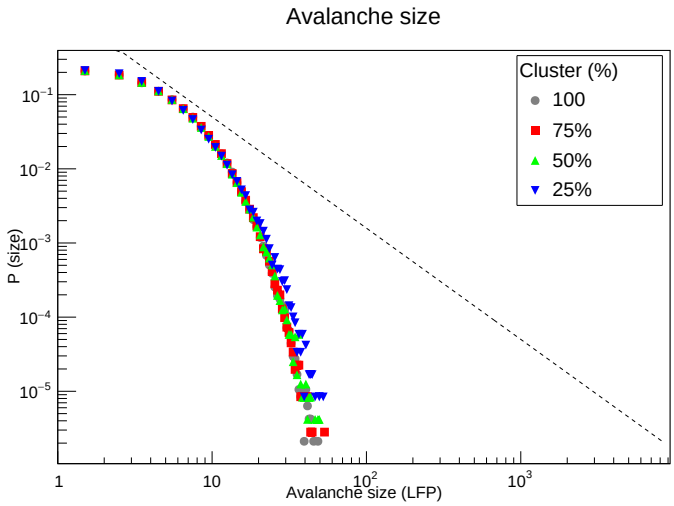

Figure 6.4: Plots of avalanche size distribution calculated using five different subsets of the clusters. The distributions do not follow the expected power law with exponent $-3/2$ (dashed line) as in Beggs and Plenz's analysis [13]. Simulations of networks of 2000 neurons, clusters of 20 neurons.

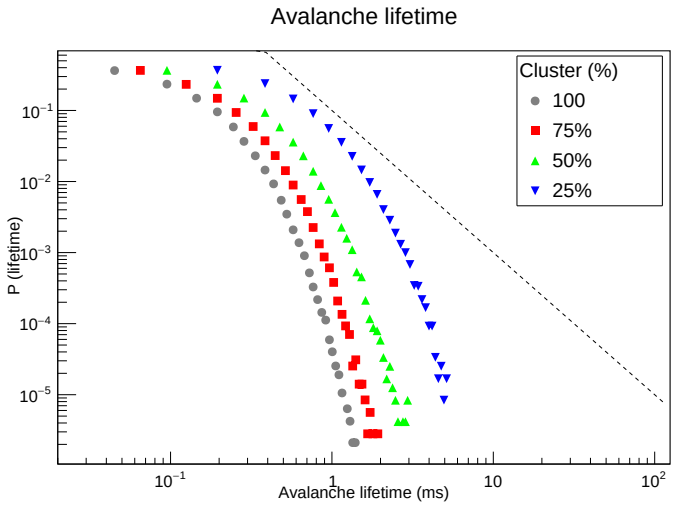

Figure 6.5: Plots of avalanche size distribution calculated using five different subsets of the clusters. The distributions do not follow the expected power law with exponent -2 (dashed line) as in Beggs and Plenz's analysis [13]. Simulations of networks of 2000 neurons, clusters of 20 neurons.

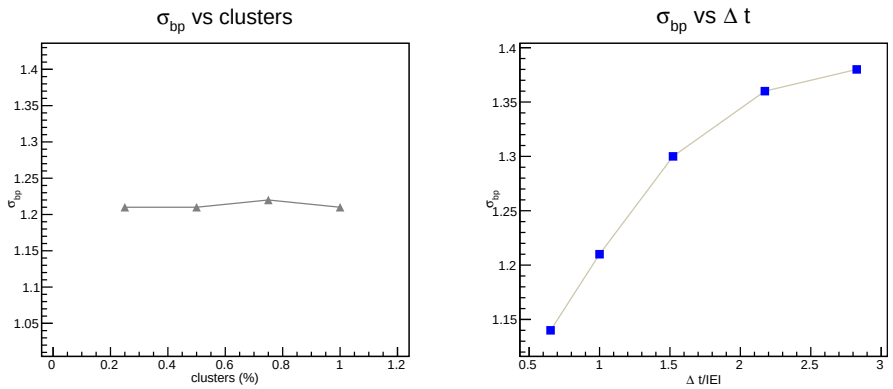

Figure 6.6: Left: σ_{bp} as a function of the fraction of clusters; σ_{bp} is approximately constant. Measures performed taking the IEI as bin size. Right: σ_{bp} as a function of the binning interval; σ_{bp} increases with increasing binning interval; the x axis gives the binning interval as a multiple of the IEI.

6.3 Branching parameter

The branching parameter has been measured for each choice of the bin size and, as can be seen in figure 6.6, it has been found to be an increasing function of the binning interval. Using the IEI to bin the data, σ_{bp} has been found to be $\sigma_{br} \approx 1.2$, which is the same value found for up and up-down state using both the direct and the subset method. The value is far from the critical value $\sigma_{bp} = 1$ measured by Beggs and Plenz. The branching parameter has also been measured as a function of the fraction of clusters analyzed; the analysis, as can be seen in figure 6.6, shows that σ_{bp} does not depend on the fraction of clusters.

6.4 Conclusions

With respect to up states, the clustering method led to the same results than both the direct and the subset method. The analysis of down states has not been performed since, as we have seen, during down states membrane potentials are, on average, highly polarized and, consequently, cluster potentials are always below the threshold. As for the analysis of up-down states, it coincide with the analysis of up states.

In the first chapter we saw that signals recorded by the electrode array consisted of long quiet times, of the order of seconds, interrupted by bursts of activity that lasted ≈ 100 ms, and that LFPs were recorded only during these active periods. This suggests that, in our analysis, up states could be associated to the active periods of the cortical networks, while down states could be associated to the quiet periods. Nevertheless, it is useful to

remember than the durations of the states are very different; in fact, our systems, as can be seen in figure 6.1, spends more time in up states than in down states, and up states are not quick bursts of activity but stable states that lasts for several seconds.

The last consideration is about the clustering procedure. It is useful to remark that our network has no spatial structure, so that the clustering of neurons does not refer to the fact that the neurons closest to each other are grouped together; in fact, neurons are grouped together completely at random.

Chapter 7

Discussion

In this work we investigated the concept of criticality in neuronal networks and, in particular, the difference between the methods used to detect criticality in the experimental analysis and the methods used to detect it in theoretical models. In our study, we focused particularly on the concept of neuronal avalanche, which plays a fundamental role in the study of neuronal networks. One of the reasons why neuronal avalanches are so important in the study of brain activity lies in the fact that they provided a link between neuronal activity and Self-Organized Criticality; in fact their size and lifetime distributions were found to follow a power law, which led to the suggestion that the brain self-organizes itself in a critical state at the boundary between being almost dead and being fully epileptic [13].

Neuronal avalanches are defined in different ways depending on whether they refer to experimental data or to data from theoretical simulations; this is due to the fact that, while in theoretical simulations we can get all the information we need about the system, the information we can obtain from experiments is always partial. In fact, data from a typical experiment consist only of a time series of events, that can be LFPs as in Beggs and Plenz's experiment [13] or other coarse measures of neural activity [42]. In order to detect the beginning and the end of each avalanche, temporal binning is applied to the sequence of events; this method leads to binning-dependent avalanches, i.e. avalanches whose sizes and lifetimes depend on the bin size. The size and lifetime distributions of such binning-dependent avalanches have been observed to follow a power law [13], which is typical of self-organized critical systems.

The same scale-free behavior of size and lifetime distributions observed in networks of real neurons was also reproduced by the Millman model [29], supporting the idea that networks of neurons are poised at criticality. However, despite the analogies, in the Millman model the detection of avalanches does not require any temporal binning but is based on causality: it is not important when a neuron has fired, but what has caused it to fire. Of course,

such a definition of avalanche requires an amount of information that cannot be obtained from experimental recordings.

The critical behavior of neuronal networks was observed in real networks using binning-dependent avalanches and in simulated networks using "causal" avalanches; in this study we analyzed the data from theoretical simulations of the Millman model with the same methods used in the experimental analysis; in other words, we applied the temporal binning to the data from theoretical simulations. We expected to find the same critical behavior observed when analyzing the data with the "causal" method; this could have supported the validity of the binning method as a way to investigate the critical properties of neuronal networks and the hypothesis that the brain operates at, or close to criticality.

Our analysis shows that, when causality is removed, the critical behavior is lost; in fact, when avalanches were detected applying the temporal binning, their size and lifetime distributions did not follow a power law anymore, regardless of the choice of the bin size. The only exception was represented by down state, whose size distribution was shown to follow a power law for small sizes, the same result found using the "causal" method; however, this is a consequence of the low spiking activity typical of down states, which causes causal and binning-dependent avalanches to be approximately the same for a wide range of bin sizes. Furthermore, the power law behavior exhibited by down state is unexpected and requires further investigation since, according to both analytical calculations and numerical simulations [29], down states are not critical.

Besides the study of avalanche distributions, another widely used method to test if the brain is in a self-organized critical state is the measure of the branching parameter σ. As in the case of avalanches, the branching parameter is defined in different ways depending on whether it refers to experimental data or to data from theoretical simulations; in fact, since the way the branching parameter is defined depends on the way avalanches are defined, in the experimental analysis σ is binning-dependent, while in theoretical models it is "causal".

The binning-dependent branching parameter was found to be close to the critical value $\sigma = 1$ for a specific choice of the bin size, the average interevent interval (IEI). Beggs and Plenz, who made this measure, suggested that the IEI was the specific bin size to be used in neural data [13]. The branching parameter was found to be $\sigma \approx 1$ also in simulations of the Millman model, with regard to up states, while it was found to be $\sigma \approx 0$ in down states; however, in the Millman model σ is "causal", while in in Beggs and Plenz's experiment it is binning dependent.

In this work, we measured the binning-dependent branching parameter of simulations of the Millman model. We expected to find, with regard to up states and with the IEI set as bin size, the same, critical value given by the measure of the "causal" branching parameter. This could have supported

both the validity of the binning procedure and the choice of the IEI as the correct bin size to be chosen for the binning of neural data; furthermore, it could have supported the hypothesis that the brain organizes itself in a critical state.

Our analysis shows that, as in the case of avalanches, when causality is not taken into account, the critical behavior is no longer observed. In fact, the binning-dependent branching parameter of up states was found to be greater than the critical value $\sigma = 1$ not only when the IEI was set as bin size, in which case it was found to be $\sigma \approx 1.2$, but also for a wide range of values around the IEI. Furthermore, the results given by the analysis of down states were very similar to the ones of up states, contrary to what happened with the "causal" branching parameter.

Our results show that the phrase "neuronal avalanche" can refer to different entities, depending on whether it concerns real networks or theoretical models, and that not only are such entities defined in different ways, but they also provide different descriptions of the same data set. Furthermore, the fact that the critical behavior of the Millman model is lost when data from numerical simulations are analyzed with the binning method raises some questions about the validity of the binning method as a way to investigate the critical properties of neuronal networks: what is the meaning of the neuronal avalanches observed by Beggs and Plenz? Do they show that Self-Organized Criticality is the underlying mechanism governing brain dynamics or are they just a consequence of the methods of experimental analysis?

A possible objection that could be raised to this work is the fact that the methods we used to detect binning dependent avalanches in networks of simulated neurons did not reproduce the experimental conditions in a realistic way. In fact, although we tried to simulate such conditions dividing the network into clusters and analyzing only a fraction of the system, the signal from each cluster (cluster potential) was very different from a local field potential (LFP), that is what is measured in real experiments; furthermore, the avalanches we detected are different from the avalanches detected in real experiments, as shown by the fact that the cutoff of size distribution did not change when only a fraction of the system was analyzed. A possible explanation is the fact that the number of neurons in a cluster is much smaller than the number of neurons that contribute to an LFP; of course, running simulations with a number of neurons comparable to the one of real networks is beyond our computational capacities, but it could be interesting to analyze how the size of the network affect the shape of cluster potentials, in order to see if the signal from bigger clusters becomes more similar to an LFP signal. This is a problem that we leave for further investigation.

Another objection that could be raised is the fact that the Millman model does not reproduce in a realistic way the behavior of neuronal networks; this could be the reason, or one of the reasons why experimental conditions could not be reproduced realistically. In fact, we simulated networks with

no spatial structure, and one of the consequences is that the clustering of neurons does not refer to the fact that the neurons closest to each other were grouped together; on the contrary, neurons were grouped together completely at random. For this reason, it would be interesting to analyze a spatially explicit version of the model, where the network has an underlying spatial structure and synaptic connections are built taking such a structure into account. However, this is a much more complicated problem that we leave for further investigation, in the hope that it could cast some light on the questions raised above.

Appendix

Receiver Operating Characteristic curve

A common signal processing problem is the one of deciding whether an observed waveform has been produced by the noise alone or by the signal plus the noise. Let us consider a physical measurement that consists of a waveform $x = \{x(t) : t \in [0, T]\}$ recorded over a time interval T, and let us call H the hypothesis that the waveform is given by the noise alone and K the hypothesis that it is given by the signal plus the noise. In order to decide between the two hypothesis, a threshold can be introduced; the signal is then declared to be present only if, for some time $t \in [0, T]$, $x(t)$ is found to be above the threshold. In this procedure, two types of errors can be made: a signal can be missed and noise can be mistaken for a signal. The frequency of such errors depends on the threshold value.

For a given threshold value x_{th}, we can define the critical region $\Re = \{x : x(t) > x_{th} \text{ for some } t \in [0, T]\}$; when a waveform is in the critical region the signal is declared to be present. Let us assume that the statistical distributions of x under the hypothesis H and K are known (this is true when the signal has a known form and the noise statistics is known, as in the case of Beggs and Plenz's experiment). We can then write the probability of false alarm as $P_{FA} = P(\Re \mid H)$ and the probability of correct detection as $P_D = P(\Re \mid K)$. Since both probabilities depend on x_{th}, we can plot P_D as a function of P_{FA} for all possible values of the threshold. Such a plot is called the receiver operating characteristic curve (see figure 1).

The ROC curve depicts the trade-off between a small number of false alarms and a small number of misses. The curve starts at the point $(0, 0)$ in the ROC space and ends at $(1, 1)$. The former corresponds to $x_{th} \longrightarrow +\infty$, which results in no false alarms and no correct detections; the latter corresponds to $x_{th} \longrightarrow -\infty$, which results in no misses and a large number of false alarms. The diagonal line in figure 1 corresponds to chance performance ($P_D = P_{FA}$) while the point $(0, 1)$ in the ROC space represents the best possible situation, where no false alarms and no misses occur. In general, the higher the ROC curve lies above the diagonal line, the better predictions it gives. Therefore, the threshold value can be chosen as the one that corresponds to the point of the ROC curve that is more distant (in the

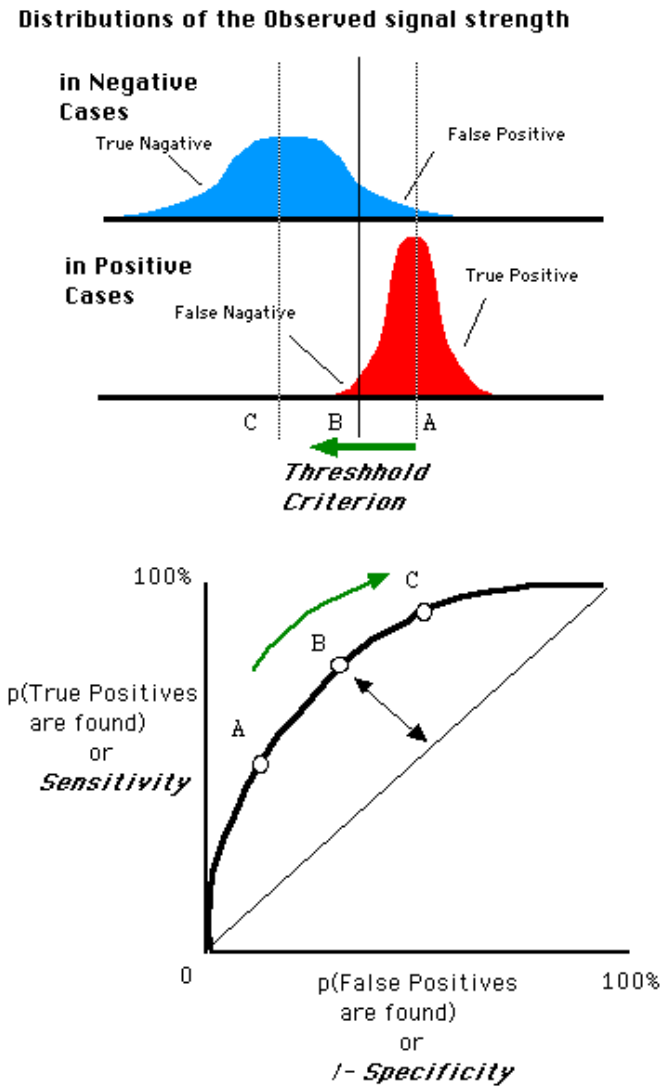

Figure 1: Example of an ROC curve. Upper figure: noise distribution (blue) and signal distribution (red). Lower figure: ROC curve for the distributions in the upper figure; the diagonal line corresponds to chance performance ($P_D = P_{FA}$). Three threshold values (A, B and C) are highlighted: the lower figure shows that the threshold value corresponding to the point in the ROC space which is more distant from the diagonal line is B.

upper direction) from the diagonal line.

Fokker-Planck formalism for integrate-and-fire models

Let us consider a general integrate-and-fire model whose dynamics is given by the equation

$$\tau \frac{dV}{dt} = -(V - V_r) + RI \ , \tag{1}$$

where V_r is the resting potential and RI is the synaptic current. Let us assume (this can be done under general conditions, see for instance Burkitt, 2006 [30]) that the synaptic input is described by a Poisson process $S(t)$ with Poisson parameter λ (i.e. a neuron has a probability λdt of receiving a synaptic input between t and $t + dt$). If we make the substitution $RI \longrightarrow aS(t)$, where a represents the weight of the synaptic input, we can write equation (1) as

$$V(t + dt) - V(t) = -\frac{V(t) - V_r}{\tau} dt + \frac{a}{\tau} S(t + dt) \ . \tag{2}$$

Taking the average[1] we obtain

$$\langle V(t + dt) \rangle - \langle V(t) \rangle = -\frac{\langle V(t) \rangle - V_r}{\tau} dt + \frac{a}{\tau} \lambda dt \ , \tag{3}$$

where we used the fact that $\langle S(t + dt) \rangle$, which is the average number of inputs in the interval dt, is equal to λdt. Solving for $\langle V(t) \rangle$ and imposing the initial condition $V(0) = V_r$ gives

$$\langle V(t) \rangle = V_r e^{-t/\tau} + \big(V_r + a\lambda\big)\big(a - e^{-t/\tau}\big) \ , \tag{4}$$

that in the limit $t \longrightarrow \infty$ (which gives the equilibrium value) gives

$$\langle V(t) \rangle \xrightarrow[t \to \infty]{} V_r + a\lambda \equiv \mu \ . \tag{5}$$

In the same way we can calculate the variance $\langle V^2(t) \rangle - \langle V(t) \rangle^2$ by squaring equation (2) (at first order in dt) and taking the average, which gives

$$\langle V^2(t) \rangle - \langle V(t) \rangle^2 \xrightarrow[t \to \infty]{} \frac{a^2 \lambda}{\tau^2} \equiv \sigma^2 \ . \tag{6}$$

We found that, in the long time limit, the membrane potential V approaches a constant value μ, around which it fluctuates with variance σ. This suggests that the membrane potential could be treated as an Ornstein-Uhlenbeck process [30] of the form

$$\tau \frac{dV}{dt} = -(V - \mu) + \sigma \sqrt{2\tau} \xi(t) \ , \tag{7}$$

[1] The average of the time-dependent random variable $V(t)$ can be computed running the process for a large number of times up to the instant t.

where $\xi(t)$ is a Gaussian white noise. In fact, this is a continuous normal Markov process whose mean and variance approach the values μ and σ in the long time limit. The net effect of this calculations is that the synaptic current RI in equation (1) has been approximated by an average part plus a fluctuating Gaussian part

$$RI = (\mu - V_r) + \sigma\sqrt{2\tau}\xi(t) \ . \tag{8}$$

Fokker-Planck equation for the Millman model

In order to write down the Fokker-Planck equation for the Millman model we need to approximate the synaptic current on the right-hand side of equation (3.6) by an average part plus a Gaussian part, as it was done in equation (8). That is, we need to write

$$R\sum_i I_e^i(t) + R\sum_j\sum_k H\big(p_r U_k(t_s^j - \zeta)I_{in}^j(t)\big) = (\mu(t) - V_r) + \sigma(t)\sqrt{2\tau}\xi(t) \ , \tag{9}$$

where $\mu(t)$ and $\sigma(t)$ are the time dependent mean and variance we need to determine. The left-hand side shows that the Millman synaptic current is the sum of two currents, the one caused by external input and the one caused by internal input, each of them contributing to $\mu(t)$ and $\sigma(t)$, so that we can write

$$\begin{cases} \mu(t) = V_r + \mu_{in}(t) + \mu_e(t) \\ \sigma^2(t) = \sigma_{in}^2(t) + \sigma_e^2(t) \end{cases} \tag{10}$$

Let us begin with the external current contributions.

The external input is already described by a Poisson process with Poisson parameter f_e, therefore all we need to do is find the weight a. In order to do so, we write the change in the membrane potential $(\Delta V)_e$ due to the arrival of an external input. Let us consider a time interval $\Delta t \gg \tau_s$ during which there is one external input and no internal inputs. Using equation (2) we can write

$$V(t + \Delta t) - V(t) \approx -\frac{V(t) - V_r}{\tau}\Delta t + (\Delta V)_e \ , \tag{11}$$

where, remembering the form of the external current given by equation (3.5), we can approximate $(\Delta V)_e$ by

$$(\Delta V)_e = Rw_e \int_0^{\Delta t} dt e^{-t/\tau_s} \approx R\tau_s w_e \ . \tag{12}$$

Therefore, for external inputs we obtain $a = R\tau_s w_e$ and $\lambda = f_e$. Using equations (5), (6) and (10) then we find

$$\begin{cases} \mu_e = R\tau_s w_e f_e = \tau V_e f_e \\ \sigma_e^2 = \dfrac{R\tau_s^2 w_e^2 f_e}{2C} = \dfrac{\tau V_e^2 f_e}{2} \end{cases} , \tag{13}$$

where $V_e \equiv w_e \tau_s / C$.

Dealing with the external inputs is a little more complex. Let us assume that the emission of action potentials of each neuron can be described by a Poisson process with the instantaneous firing rate $f(t)$ as Poisson parameter, and let us assume that, even though the firing rate is the same for all neurons, Poisson processes relative to different neurons are uncorrelated. Then, given a neuron that can receive inputs from n other neurons, its synaptic inputs can be described by an inhomogeneous Poisson process with Poisson parameter $nf(t)$. Therefore, since the average number of internal inputs per neuron of the Millman model is n_s, we can describe the internal synaptic inputs as a Poisson process with parameter $n_s f(t)$.

In order to obtain the weight a we need to take into account the fact that the release of a neurotransmitter occurs with probability $p_r U(t)$, where $U(t)$ is given by equation (3.3). Using the definition of the mean synaptic utility $u(t) \equiv \langle U(t) \rangle$, were the average is taken over all release sites of all synapses, and following the same method used for the external inputs we find $a = R\tau_s w_{in} p_r n_r u$, where n_r is the number of release sites per synapse. We can then write

$$\begin{cases} \mu_{in}(t) = R\tau_s w_{in} p_r n_r u n_s f(t) = \tau V_{in} u n_s f(t) \\ \sigma_{in}^2(t) = \dfrac{R(\tau_s w_{in} p_r n_r u)^2 n_s f(t)}{2C} = \dfrac{\tau V_{in}^2 n_s f(t)}{2} \end{cases} , \tag{14}$$

where $V_{in} \equiv w_{in} \tau_s p_r n_r / C$. Finally, substituting in equation (10) we find

$$\begin{cases} \mu(t) = V_r + \tau V_{in} u n_s f(t) + \tau V_e f_e \\ \sigma^2(t) = \dfrac{\tau (V_{in} u)^2 n_s f(t)}{2} + \dfrac{\tau V_e^2 f_e}{2} \end{cases} . \tag{15}$$

Substituting in equation (3.12) we obtain the Fokker-Planck equation for the Millman model.

Time derivative of the mean synaptic utility

The mean synaptic utility is defined as $u(t) \equiv \langle U(t) \rangle$. Every time that a neurotransmitter is released by a given site, the $U(t)$ factor of the site is set to zero. This happens at the rate $k_D = u p_r f$, which is called rate of depression. The site then recovers with an average frequency

$$k_R = \frac{d\langle U(t) \rangle}{dt} = \frac{1 - \langle U(t) \rangle}{\tau_R} = \frac{1 - u}{\tau_R} ,$$

where it has been used the fact that

$$\frac{dU(t)}{dt} = \frac{1 - U(t)}{\tau_R} .$$

The rate k_R is called rate of recovery. The derivative of the mean synaptic utility is given by the difference between rate of recovery and rate of depression, that is

$$\frac{du}{dt} = \frac{1-u}{\tau_R} - up_r f \ . \tag{16}$$

Branching parameter

Let us consider a stationary state $p(V, \infty)$ and let us call the stationary mean synaptic utility and firing rate at that state u^* and f^*. From equations (3.18), (3.14) and (3.16) we get:

$$\begin{cases} \sigma = -\dfrac{n_s(uV_{in})^2}{2}\dfrac{\partial P(V_{th},\infty)}{\partial V} \\ f^* = -\dfrac{(V_{in}u^*)^2 n_s f(t) + V_e^2 f_e}{2}\dfrac{\partial P(V_{th},\infty)}{\partial V} \end{cases} . \tag{17}$$

Solving the first equation for $\partial P(V_{th}, \infty)/\partial V$ and substituting in the second one gives

$$\sigma = \frac{n_s V_i n^2 f^*}{V_e^2 f_e (1 + p_r \tau_r f^*)^2 + n_s V_{in}^2 f^*} \ , \tag{18}$$

where it has been made the substitution

$$u^* = \frac{1}{1 + p_r \tau_R f^*} \ ,$$

that comes from equation (16) at the stationary state.

Bibliography

[1] Bak, P., Tang, C., Wiesenfeld, K., Self-Organized Criticality: an explanation of $1/f$ noise, *Physical Review Letters*, 59, 381, 1987.

[2] Bak, P., Tang, C., Wiesenfeld, K., Self-Organized Criticality, *Physical Review A*, 38, 364, 1988.

[3] Bak, P., *How nature works: the science of self-organized criticality*, Springer, 1996.

[4] Bak, P., Tang, C., Earthquakes as a Self-Organized Critical Phenomenon, *Journal of geophysical research*, 94, 635, 1989.

[5] Per Bak, P., Christensen, K., Danon, L., Scanlon, T., Unified Scaling Law for Earthquakes, *Phys. Rev. Lett.*, 88, 178501, 2002. Bak, P., Tang, C., Earthquakes as a Self-Organized Critical Phenomenon, *Journal of geophysical research*, 94, 635, 1989.

[6] Malamud, B. D., Morein, G., Turcotte, D. L., Forest Fires: An Example of Self-Organized Critical Behavior, *Science*, 281, 1840, 1998.

[7] Lu, E. T., Hamilton, R. J., Avalanches and the distribution of solar flares, *The Astrophysical Journal*, 380, L89, 1991.

[8] Mora, T., Bialek, W., Are biological systems poised at criticality?, *Journal of statistical physics*, 144, 268, 2011.

[9] Furusawa, C., Kaneko, K., Adaptation to optimal cell growth through self-organized criticality, *Phys Rev Lett*, 108, 208103, 2012.

[10] Chen, X., Dong, X., Beer, A., Swinney, H., Zhang. H., Scale-invariant correlations in dynamic bacterial clusters, *Phys Rev Lett*, 108, 148101, 2012.

[11] Krotov, D., Dubuis, J. O., Gregor, T., Bialek, W., Morphogenesis at criticality, *Proceedings of the National Academy of Sciences*, 111, 3683, 2014.

[12] Nykter, M., et al., Gene expression dynamics in the macrophage exhibit criticality, *Proc Nat Acad of Sci*, 105, 1897, 2008.

[13] Beggs, J. M., Plenz, D., Neuronal avalanches in neocortical circuits, *J. Neurosci.*, 23, 11167, 2003.

[14] Jimbo, Y., Robinson, H. P. C., Propagation of spontaneous synchronized activity in cortical slice cultures recorded by planar electrode arrays, *Bioelettrochemistry*, 51, 107, 2000.

[15] Plenz, D., Aertsen, A., Current source density profiles of optical recording maps: a new approach to the analysis of spatio-temporal neural activity patterns, *Eur J Neurosci*, 5, 437, 1993.

[16] Arieli, A., *Novel strategies to unravel mechanisms of cortical function: from macro-to micro-electrophysiological recordings*, Springer, 1992.

[17] Bove, M, Genta, G., Verreschi, G., Grattarola, M., Characterization and interpretation of electrical signals from random networks of cultured neurons, *Technol Health Care*, 4, 77, 1996.

[18] Gabbiani, F., Koch, C., *Principles of spike train analysis*, MIT, 1998.

[19] Madisetti, V., K., Williams, D., B., *The digital signal processing handbook*, CRC PRESS and IEEE PRESS, 1997.

[20] Plenz, D., Aertsen A., Neural dynamics in cortex-striatum cocultures—II. Spatiotemporal characteristics of neuronal activity, *Neuroscience*, 70, 893, 1996.

[21] Zapperi, S., Baekgaard. L. K., Stanley, H. E., Self-organized branching processes: mean field theory for avalanches, *Phys. Rev. Lett.*, 75, 4071, 1995.

[22] Harris, T., *The theory of branching processes*, Springer, Courier corporation, 2002.

[23] de Carvalho, J. X., Prado, C., P., Self-organized criticality in the Olami-Feder-Christensen model, *Phys. Rev. Lett.*, 84, 4006, 2000.

[24] Dayan, P., Abbott, L. F., *Theoretical neuroscience - computational and mathematical modeling of neural systems*, MIT Press, 2001.

[25] Kandel, E. R., Schwartz, J. H., Jessell, T. M., Siegelbaum, S. A., Hudspeth, A., J., *Principles of neural science*, Mac Graw Hill, 2012.

[26] Hammer, G. D., McPhee, S. J., *Pathophysiology of desease*, Mac Graw Hill, 2014.

[27] Abbott, L. F., Lapicque's introduction of the integrate-and-fire model neuron (1907), *Brain research bulletin*, 50, 303, 1999.

[28] Hodgkin, A. L., Huxley, A. F., A quantitative description of membrane current and its application to conduction and excitation in nerve, *J. Physiol.*, 117, 500, 1952.

[29] Millman, D., Mihalas, S., Kirkwood, A., Niebur, E., Self-organized criticality occurs in non-conservative neuronal networks during 'up' states, *Nature Physics*, 6, 801, 2010.

[30] Burkitt, A. N., A review of the integrate-and-fire neuron model: I. Homogeneous synaptic input, *Biol. Cybern.*, 95, 1, 2006.

[31] Brunel, N, Dynamics of sparsely connected networks of excitatory and inhibitory spiking neurons, *Journal of computational neuroscience*, 8, 183, 2000.

[32] Brunel, N., Hakim, V., Fast global oscillations in networks of integrate-and-fire neurons with low firing rates, *Neural Comput*, 11. 1621, 1999.

[33] Südhof, T. C., The synaptic vesicle cycle, *Annu. Rev. Neurosci.*, 27, 509, 2009.

[34] Brette, R. et al., Simulation of networks of spiking neurons: a review of tools and strategies, *J. Comput. Neurosci.*, 23, 349, 2007.

[35] Südhof, T. C., The synaptic vesicle cycle, *Annu. Rev. Neurosci.*, 27, 509, 2004.

[36] Dobrunz, L. E., Stevens, C. F., Heterogeneity of release probability, facilitation, and depletion at central synapses, *Neuron*, 18, 995, 1997.

[37] Plenz, D., Kitai, S. T., Up and down states in striatal medium spiny neurons simultaneously recorded with spontaneous activity in fast-spiking interneurons studied in cortex-striatum-substantia nigra organotypic cultures, *J. Neurosci.* 18, 266, 1998.

[38] Lampl, I., Reichova, I., Ferster, D., Synchronous membrane potential fluctuations in neurons of the cat visual cortex, *Neuron*, 22, 361, 1999.

[39] Compte, A., Reig, R., Descalzo, V. F., Harvey, M. A., Puccini, G. D. et al., Spontaneous high-frequency (10–80 hz) oscillations during up states in the cerebral cortex in vitro, *J Neurosci*, 17, 13828, 2008.

[40] Wallace, E., Benayoun, M., van Drongelen, W., Cowan, J., Emergent Oscillations in Networks of Stochastic Spiking Neurons, *PLoS ONE*, 6, e14804, 2011.

[41] Hidalgo, J., Seoane, L. F., Cortés, J. M., Muñoz, M. A., Stochastic Amplification of Fluctuations in Cortical Up-States, *PLoS ONE*, 8, e40710, 2012.

[42] Shriki, O., Alstott, J., Carver, F., Holroyd, T., Henson, R. N., Smith, M. L. et al., Neuronal Avalanches in the resting MEG of the human brain, *J. Neurosci.*, 33, 7079, 2013